

Cell Stem Cell

Membrane tension gates ERK-mediated regulation of pluripotent cell fate

--Manuscript Draft--

| | |
|------------------------------|---|
| Manuscript Number: | CELL-STEM-CELL-D-20-00734R2 |
| Full Title: | Membrane tension gates ERK-mediated regulation of pluripotent cell fate |
| Article Type: | Research Article |
| Keywords: | Embryonic Stem cells; Membrane tension; ERK; Endocytosis |
| Corresponding Author: | Kevin J Chalut, Ph.D. University of Cambridge Cambridge, UNITED KINGDOM |
| First Author: | Henry De Belly |
| Order of Authors: | Henry De Belly Aki Stubb, PhD Ayaka Yanagida Celine Labouesse Philip H Jones Ewa K Paluch Kevin J Chalut |
| Abstract: | <p>Cell fate transitions are frequently accompanied by changes in cell shape and mechanics. Yet how cellular mechanics affects the instructive signalling pathways controlling cell fate is poorly understood. To probe the interplay between shape, mechanics, and fate, we use mouse embryonic stem (ES) cells, which change shape as they undergo early differentiation. We find that shape change is regulated by a β-catenin mediated decrease in RhoA activity and subsequent decrease in the plasma membrane tension. Strikingly, preventing a decrease in membrane tension results in early differentiation defects in ES cells and gastruloids. Decreased membrane tension facilitates endocytosis of FGF signaling components, which activates ERK signaling and directs exit from the ES cell state. Increasing Rab5a-facilitated endocytosis rescues defective early differentiation. Thus, we show that a mechanically-triggered increase in endocytosis regulates early differentiation. Our findings are of fundamental importance for understanding how cell mechanics regulates biochemical signaling, and therefore cell fate.</p> |

Title: Membrane tension gates ERK-mediated regulation of pluripotent cell fate

Authors: Henry De Belly^{1, 2, 3}, Aki Stubb³, Ayaka Yanagida^{2, 4}, Céline Labouesse², Philip H. Jones⁵, Ewa K. Paluch^{1, 3, *}, Kevin J. Chalut^{2, *}

Affiliations:

¹ MRC Laboratory for Molecular Cell Biology, University College London, Gower Street, London, WC1E 6BT, UK.

² Wellcome/MRC Cambridge Stem Cell Research Institute, Puddicombe Way, University of Cambridge, Cambridge, CB2 0AW.

³ Department of Physiology, Development and Neuroscience, Downing Street, University of Cambridge, Cambridge, CB2 3DY, UK.

⁴ Living Systems Institute, University of Exeter, Exeter, EX4 4QD, UK.

⁵ Department of Physics & Astronomy, University College London, Gower Street, London, WC1E 6BT, UK.

Lead contact: kc370@cam.ac.uk

(*) Correspondence: ekp25@cam.ac.uk, kc370@cam.ac.uk

Summary:

Cell fate transitions are frequently accompanied by changes in cell shape and mechanics. Yet how cellular mechanics affects the instructive signalling pathways controlling cell fate is poorly understood. To probe the interplay between shape, mechanics, and fate, we use mouse embryonic stem (ES) cells, which change shape as they undergo early differentiation. We find that shape change is regulated by a β -catenin mediated decrease in RhoA activity and subsequent decrease in the plasma membrane tension. Strikingly, preventing a decrease in membrane tension results in early differentiation defects in ES cells and gastruloids. Decreased membrane tension facilitates endocytosis of FGF signaling components, which activates ERK signaling and directs exit from the ES cell state. Increasing Rab5a-facilitated endocytosis rescues defective early differentiation. Thus, we show that a mechanically-triggered increase in endocytosis regulates early differentiation. Our findings are of fundamental importance for understanding how cell mechanics regulates biochemical signaling, and therefore cell fate.

Introduction:

The integration of mechanics with cell signaling has a crucial impact on cell function. A number of studies have highlighted the importance of sensing the mechanical properties of the extracellular environment in developmental morphogenesis (Heisenberg and Bellaïche, 2013; Koser et al., 2016), immunity (Solis et al., 2019), tumorigenesis (Halder et al., 2012), and wound healing (Razzell et al., 2014). The influence of extracellular mechanical cues is also emerging as a key player in tissue homeostasis (Gudipaty et al., 2017; Pepe-Mooney et al., 2019; Yui et al., 2018) and stem cell function and fate choice (Engler et al., 2006; Przybyla et al., 2016; Segel et al., 2019; Totaro et al., 2017). Most of these studies have focused on how the mechanics of the environment, in particular substrate stiffness, affects cell function.

At the same time, several studies suggest that changes in cell shape correlate with changes in signaling and fate. For example, it was shown that serum response factor signaling is regulated by spreading in epidermal stem cells (Connelly et al., 2010), and Stat3 signaling is linked to spreading in embryonic stem cells (Murray et al., 2013). It was also shown that the extent of spreading may affect fate choice in mesenchymal stromal cells (McBeath et al., 2004). Importantly, cell shape is controlled by forces exerted by the cytoskeleton on the cell surface; thus, it is a direct readout of intrinsic cell mechanics (subsequently cell mechanics, reviewed in (Clark et al., 2014; Heisenberg and Bellaïche, 2013)). Therefore, cell mechanics and substrate stiffness could both affect signaling. However, cell and substrate mechanics are often coupled (Tee et al., 2011). As a result, studying the effects of cell mechanics on cell function is challenging and the mechanisms by which the intrinsic mechanical properties of a cell could affect signaling remain elusive.

An excellent model system to investigate mechanical signaling in the context of a well-defined fate transition is embryonic stem (ES) cells. Mouse ES cells possess the ability to produce all tissues, a property called ‘pluripotency’ (Avior et al., 2016; Chen et al., 2016). These cells can be maintained indefinitely in a ‘naïve’ state (Evans and Kaufman, 1981; Ying et al., 2008) and ushered through distinct phases of pluripotency (Kalkan et al., 2017) including the highly characterized first stage of differentiation, exit from naïve pluripotency (Kalkan et al., 2017; Mulas et al., 2019). The signaling requirements of exit from naïve pluripotency are well-understood; the

process has been shown to be primarily driven by FGF/ERK signaling (Kunath et al., 2007; Nett et al., 2018). Interestingly, it was recently shown that ES cells are not sensitive to external mechanical cues (Verstreken et al., 2019); yet ES cells display a striking shape change, from round to spread, as they exit naïve pluripotency (Chalut and Paluch, 2016), indicative of changes in cell mechanics. Thus, mouse ES cells constitute a particularly appropriate model system to dissect the role of cell mechanics in signaling in a well-defined fate transition.

Here, we show that the shape change observed in early ES cell differentiation is driven by a reduction in effective membrane tension. We demonstrate that this change in membrane tension is regulated by the key pluripotency factor β -catenin (Wray et al., 2011). We further show that the decrease in membrane tension accompanying early differentiation leads to increased endocytosis of fibroblast growth factor (FGF) signaling components. This results in increased activity of extracellular signal-regulated kinase (ERK), which is necessary for exit from naïve pluripotency. Altogether, our study unveils a key mechanism whereby changes in cellular mechanics regulate the signaling that drives fate transitions.

Results:

Early differentiation of ES cells correlates with membrane tension reduction and spreading.

To study the interplay between cell shape and cell fate change, we first asked whether cell shape correlates with fate during the early stages of exit from naïve pluripotency. ES cells were cultured on gelatin coated plates and maintained in N2B27 medium supplemented with the MEK/ERK inhibitor PD0325901, the GSK3 inhibitor/ β -catenin agonist CHIRON, and Leukemia inhibitory factor (culture medium known as 2i+L) (Mulas et al., 2019). Exit from naïve pluripotency was initiated by withdrawing the inhibitors and culturing cells in N2B27 medium alone. After 24h in N2B27 (T24), cells displayed a mixture of shapes, with most cells already flat and spread, and some still round and in colonies (Figure 1A & S1A). This heterogeneity is consistent with previously described asynchrony in exit from naïve pluripotency (Kalkan et al., 2017). To identify a potential correlation with cell fate, we fixed the cells and, in cells of different shapes, quantified the expression of Nanog, a marker of naïve pluripotency, and Otx2, a transcription factor upregulated in cells that have exited naïve pluripotency (Kalkan et al., 2017). We found that Nanog

levels were significantly higher, and Otx2 significantly lower, in round cells as compared to spread cells (Figure 1B, C), thus establishing a correlation between cell shape and exit from naïve pluripotency.

We next characterized the dynamics of cell spreading during exit from naïve pluripotency. To do this, we captured time-lapse images of ES cells stably expressing LifeAct-GFP to visualize filamentous actin (Movie S1). We observed that, prior to spreading, the cells displayed a phase of intense blebbing (Figure S1B-D). Notably, blebbing is often a sign of low membrane-to-cortex attachment (Charras and Paluch, 2008), a key mechanical parameter controlling the apparent tension of the plasma membrane. Apparent membrane tension (subsequently referred to as “membrane tension”) depends on the in-plane tension of the lipid bilayer and on membrane-to-cortex attachment, and is a measure of the resistance of the plasma membrane to deformations (Pontes et al., 2017a). As such, it is a major regulator of cell shape (Diz-Muñoz et al., 2013). Furthermore, in our SEM images T48 cells displayed more surface membrane folds and reservoirs compared to naïve cells (Figure 1A & S1A), suggesting differences in membrane tension (Pontes et al., 2017a).

We next asked whether exit from naïve pluripotency is associated with a change in membrane tension. To address this, we employed a tether pulling assay using optical tweezers (Movie S2, Figure 1D, E & S1E), where the force exerted on the bead by the membrane tether (the “trap force”) is a direct readout of membrane tension (Diz-Muñoz et al., 2013). We found that ES cells significantly decrease their membrane tension as they exit naïve pluripotency (Figure 1E). Moreover, at T24, when cell populations display mixed morphologies, round cells had a significantly higher membrane tension than blebbing and spread cells. This is consistent with previous studies showing that cell spreading is facilitated by decreased membrane tension (Pontes et al., 2017b; Raucher and Sheetz, 2000). Therefore, we conclude that cell spreading during exit from naïve pluripotency occurs concomitantly with a decrease in plasma membrane tension.

Membrane tension has been shown to be regulated largely by linkers between the plasma membrane and the underlying actomyosin cortex, such as Ezrin-Radixin-Moesin (ERM) and Myosin I proteins (Nambiar et al., 2009; Pontes et al., 2017a). To narrow the list of potential

regulators of membrane tension, we checked the expression of genes encoding for linker proteins in ES cells and in their *in vivo* counterpart, the pre-implantation epiblast, using a published dataset (Boroviak et al., 2015). We found that ERM proteins, and in particular Ezrin, were up to 10 times more expressed than Myosin I proteins. We thus focused on ERM proteins, which are activated by phosphorylation (Gautreau et al., 2000). At the population level we found that the level of phosphorylated ERM (pERM) was sharply decreased after 2i+L removal (Figure 1F & S1F). We confirmed these results using immunostaining of T16 cells, which showed that spread cells have lower levels of pERM than round cells (Figure S1G-J).

The decrease in membrane tension during early differentiation is induced by a β -catenin mediated decrease in ERM phosphorylation.

We then investigated which pluripotency-regulating signaling pathway is primarily responsible for the decrease in pERM upon removal of ES cell media. We first reduced the medium to the minimal signaling environment necessary to maintain naïve pluripotency (2i) (Ying et al., 2008). We then separately removed PD0325901 (PD03) and CHIRON (CHIR) from 2i to study the effects of MEK/ERK activation and GSK3b activation, respectively. We found that, while PD03 removal did not lead to a pERM & decrease, CHIR removal resulted in a rapid and significant decrease in pERM and decrease in membrane tension (Figure S2A-C), pointing to a role for GSK3b signaling in regulating pERM levels. Given that increased GSK3b activation leads to β -catenin degradation (Liu et al., 2002), and that β -catenin is partly localized at the plasma membrane, we asked whether β -catenin depletion would lead to a decrease in pERM and subsequent decrease in membrane tension. To address this question, we measured pERM levels and membrane tension in β -catenin knockout (KO) ES cells (Wray et al., 2011) and found that both were significantly lower compared to wild type (WT) ES cells (Figure 2A, B). These results suggest that GSK3b-driven β -catenin degradation mediates a decrease in pERM, which in turn controls membrane tension and cell shape during exit from naïve pluripotency.

β -catenin regulates ERM phosphorylation by modulating RhoA activity.

We next investigated the link between β -catenin and ERM phosphorylation. We speculated that, given that the known link between RhoA activity and the cadherin-catenin complexes (Arnold et

al., 2017) and that active RhoA is one of the key activators of ERMs (Matsui et al., 1998), that RhoA might connect β -catenin to ERM. To test this hypothesis, we measured RhoA activity during exit from naïve pluripotency using an active a FRET reporter and an active RhoA pull down assay and found that ES cells displayed a significant decrease in RhoA activity during exit from naïve pluripotency (Figure 2C-F & Figure S2D). Furthermore, our results show that levels of active RhoA are significantly lower in β -catenin KO cells compared to WT ES cells (Figure 2E, F).

We then used a Doxycycline-inducible ES cell line expressing a phosphomimetic, constitutively active form of RhoA to probe whether higher RhoA activity does indeed lead to higher ERM phosphorylation and thus higher membrane tension in ES cells. After Doxycycline-induction, we found that the inducible, constitutively active RhoA (iRhoA_CA) cells showed high levels of ERM phosphorylation and subsequently maintained a high membrane tension during exit from naïve pluripotency (Figure 2G, H). Taken together our findings indicate that β -catenin degradation by GSK3 leads to a decrease in RhoA activity, which drives a subsequent decrease in ERM phosphorylation and membrane tension, suggesting that RhoA activity represents a key link between β -catenin and ERM regulation.

Maintaining high membrane tension impairs early differentiation.

We then asked whether the membrane tension decrease plays a role in controlling exit from naïve pluripotency. We used both the iRhoA_CA cells and a Doxycycline-inducible ES cell line expressing a phosphomimetic, constitutively active form of Ezrin (iEZR_CA). After induction, iEZR_CA cells showed high EZR_CA expression and no growth defects (Figure S3A, B). After withdrawal of the naïve factors (2i+L), iEZR_CA and iRhoA_CA cells did not spread (Figure 3A & S3C) even at T48, and they maintained high membrane tension similar to ES cells (Figure 3B & Figure 2H). We also found that, compared to controls, iEZR_CA & iRhoA_CA cells at T24 maintained significantly higher levels of Nanog and failed to efficiently upregulate Otx2 (Figure 3C, D & S3C, D). A clonogenicity assay indicated that unlike control T48 wild type cells, iEZR_CA & iRhoA_CA cells placed back in 2i+L after 48 hours in N2B27, were able to survive and form naïve colonies with the same efficiency as naïve ES cells (Figure 3E & S3E, see Materials and Methods for details). To confirm the early differentiation phenotype, we performed RNA sequencing comparing iEZR_CA and WT ES, T24 and T48 cells. We found that iEZR_CA cells

showed a significant impairment both in loss of naïve pluripotency markers and in subsequent expression of early implantation markers (Figure 3F, G & S3I). Together, these results indicate that maintaining a high membrane tension in pluripotent cells significantly inhibits their ability to exit naïve pluripotency.

Furthermore, treating cells with methyl- β -cyclodextrin, a cholesterol-sequestering compound that increases membrane tension (Biswas et al., 2018) (Figure S3J, K), delayed exit from naïve pluripotency (Figure S3L). Conversely, treating cells with NSC 668394, an ezrin inhibitor that decreases membrane tension (Rouven Brückner et al., 2015) (Figure S3J, K), caused cells to exit naïve pluripotency more efficiently than control cells (Figure S3L). Moreover, a recent study showed that using a purely mechanical linker between actin and the plasma membrane to increase effective membrane tension also blocks exit from naïve pluripotency (Bergert et al., 2020).

To assess the developmental relevance of these findings, we used a gastruloid assay (adapted from (Baillie-Johnson et al., 2015) in which we compared the ability of iEZR_CA to form gastruloids at different stages (Figure 3H-K). We found that iEZR_CA gastruloids displayed clear morphological defects, completely failing to elongate and adopt the characteristic morphology of properly progressing gastruloids with distinct multi-axial organisation. The lack of elongation suggests major developmental defects in those gastruloids (Turner et al., 2017). We also performed morula injection of iEZR_CA and control cells at the 8-cell stage and maintained embryos in culture for two or three days, resulting in embryos which are the equivalent of developmental stages E4.5 & E5.5, respectively. We consistently observed a higher level of the naïve pluripotency marker Nanog in the iEZR_CA compared to native and control cells (Figure S4A, B), thus suggesting that high membrane tension also leads to a delay in differentiation in the embryo.

Taken together, our data strongly suggests that a pERM-controlled decrease in plasma membrane tension is essential for cell spreading and for exit from naïve pluripotency.

Membrane tension reduction, not cell spreading, is responsible for gating early differentiation.

To clarify the relative importance of cell shape change and membrane tension, we used micropatterning to control the extent of cell spreading with disks of different diameters (small: 25-50 μm or large: 100 μm). We seeded ES cells at equal densities onto both small and large micropatterns in N2B27 only. We found that in contrast to cells plated on large patterns or non-patterned surfaces, spatially-constrained T24 cells on small patterns did not change shape and maintained a rounded morphology similar to ES cells (Figure 4A, B). Spatially constrained cells at T24 maintained high levels of Nanog suggesting defects in exiting naïve pluripotency (Figure 4B, C & S4C). However, spatially constrained cells also maintained a high membrane tension (Figure 4D). Strikingly, the exit from naïve pluripotency on small micropatterns, where cells cannot spread, was rescued by knockdown of ERM (Figure 4E & S4D-G) or knockdown of Myosin I family proteins (Figure S4H, I), treatments previously shown to reduce membrane tension (Diz-Muñoz et al., 2010; Rouven Brückner et al., 2015). Together, these experiments point to the existence of positive feedback loops between membrane tension decrease and cell spreading, and indicate that it is the decrease in membrane tension, rather than cell spreading, that is required for efficient exit from naïve pluripotency.

To further test whether membrane tension regulates exit from naïve pluripotency directly, or as a result of cell spreading, we plated ES cells on either laminin or E-cadherin, where they display spread morphologies even in 2i+L (Figure 4F). Despite the fact that for cells on laminin & E-cadherin exit from pluripotency was associated with a much less pronounced spreading increase than for cells on gelatin, we still observed a similar drop in membrane tension during exit from pluripotency (Figure 4G). This further indicates that it is the decrease in membrane tension, and not the spreading directly, that is needed for efficient dismantling of naïve pluripotency.

Membrane tension regulates endocytosis levels in ES cells.

We then asked how decreased membrane tension facilitates exit from the ES cell state. We speculated that the facilitation may be through endocytosis, which is a major regulator of signaling events (Pouille et al., 2009; Sorkin and von Zastrow, 2009) and has been shown to be regulated by membrane tension (Dai and Sheetz, 1995; Thottacherry et al., 2018). First, we assessed global endocytosis levels using a fluid phase uptake assay, in which we cultured cells in presence of either fluorescent dextran or a pH-sensitive fluorescent dextran (Figure 5A). Using this assay, we found

that T24 cells displayed a significant increase in endocytosis levels once spread (Figure 5B, C & S5A, B). We next interfered with this increase using drugs known to inhibit endocytosis (Dynasore, PitStop2 & Chlorpromazine hydrochloride) (Dutta and Donaldson, 2012). We found that WT cells treated with these drugs failed to increase their endocytosis rates during exit from naïve pluripotency (Figure 5D). We next assessed whether cells with endocytosis defects could exit naïve pluripotency normally and found that these cells maintained a higher level of Nanog, and a lower level of Otx2 expression compared to controls (Figure 5E-G). Altogether, these observations suggest that endocytosis regulates exit from naïve pluripotency.

We next examined the link between the observed differentiation-induced drop in membrane tension and endocytosis. We showed that endocytosis was considerably reduced in cells expressing iEZR_CA (Figure 5H, I) and that it was increased in β -catenin KO ES cells (Figure S5C), suggesting, consistent with previous findings in other systems (Dai and Sheetz, 1995; Thottacherry et al., 2018), that high membrane tension antagonizes endocytosis. To test whether enhanced endocytosis could overcome the block in differentiation imposed by EZR_CA, we overexpressed Rab5a, a master regulator of early endosomes (Palamidessi et al., 2019), in iEZR_CA cells. Elevation of Rab5a levels has been shown to promote endocytosis (Mendoza et al., 2014; Palamidessi et al., 2019). Indeed, we found that overexpressing Rab5a increased endocytosis levels in iEZR_CA cells compared to non-transfected controls, both in ES and T24 cells without leading to growth defects (Figure 5H, I & S5D) and without lowering membrane tension (Figure S5E). Notably, Rab5a expression rescued the exit phenotype in iEZR_CA cells, restoring Nanog downregulation (Figure 5J, K) and decreasing the number of colonies surviving in a clonogenicity assay, indicative of more efficient exit from naïve pluripotency (Figure S5F). Furthermore, transfection with Rab5a also enabled downregulation of Nanog protein in spatially-constrained T24 cells (Figure S5G). These results show that increasing endocytosis levels via Rab5a overexpression allows ES cells to exit naïve pluripotency notwithstanding a high membrane tension.

Membrane tension-mediated endocytosis promotes ERK activation during early differentiation

Finally, we asked whether a specific signaling pathway related to regulation of naïve pluripotency was affected by the changes in cell mechanics and endocytosis we observed. The most obvious candidate was FGF/ERK, as it is key for exit from naïve pluripotency (Nichols et al., 2009), and its EGF/ERK counterpart been shown to be regulated by endocytosis in cancer cells (Palamidessi et al., 2019; Sorkin and von Zastrow, 2009). We thus quantified pERK levels during exit from naïve pluripotency, and observed that at all time points ERK activity was highly attenuated in the iEZR_CA cells (Figure 6A, B & S6A, B). We also confirmed a global reduction in MAPK/ERK signaling in iEZR_CA cells by RNAseq analysis of known transcriptional targets (Figure S6C). These results strongly suggest that maintaining a high membrane tension during exit from naïve pluripotency prevents ERK activation. To further test the role of ERK activity in the early differentiation impairment of the iEZR_CA cells, we treated iEZR_CA cells with the RSK inhibitor BI-D1870, which acts as an ERK activator (Nett et al., 2018). We found that this treatment was sufficient to rescue the early differentiation defects of iEZR_CA (Figure 6C, D), which we further confirmed using a clonogenicity assay (Figure S6D).

Internalization of receptors by endocytosis has been shown to influence the levels pERK activity (Palamidessi et al., 2019; Platta and Stenmark, 2011). Thus, we measured internalization of FGFR1, which is upstream of pERK in ES cells (Molotkov et al., 2017), in iEZR_CA and control cells using immunofluorescence. We found that iEZR_CA cells had less internalized FGFR1 compared to controls (Figure S6E, F), despite expressing similar protein levels (Figure S6G). We were able to increase the levels of internalized FGFR1 in iEZR_CA by over-expressing Rab5a (Figure S6E, F). We then specifically probed pERK activity at endosomes using a recently-described FRET sensor reporting on ERK activity at early endosomes (Figure 6E) (Palamidessi et al., 2019). Using live imaging, we found that pERK at endosomes sharply increased as cells spread (Figure 6E-G and S6H, Movie S3). We confirmed this with measurements in fixed cells, finding that spread T24 cells showed a higher FRET ratio compared to round T24 cells. Notably, we observed a lower FRET ratio in T24 cells where endocytosis rates were reduced chemically with dynasore or by increasing membrane tension via iEZR_CA expression (Figure 6H). Furthermore, increasing endocytosis independently of membrane tension, by expression of Rab5a in iEZR_CA cells, resulted in a FRET ratio similar to spread control cells at T24 (Figure 6H). Taken all together,

our results indicate that ERK activity, which helps disassemble naïve pluripotency, is induced by membrane tension-regulated endocytosis in cells exiting pluripotency (Figure 6I).

Discussion:

There is extensive interplay between substrate mechanics, cell mechanics, and cell function (Guilak et al., 2009). Moreover, cell shape, which is a readout of cell mechanics, is correlated with cell fate (Bellas and Chen, 2014). Because cell shape, cell mechanics and cell fate are deeply intertwined, it is challenging to disentangle them to understand specifically how cell mechanics mediates signaling. To probe the role of cell mechanics in cell fate transitions, we focused on exit from naïve pluripotency in ES cells. Interestingly, we found that it is the change in cell surface mechanics, not cell shape, that regulates early differentiation. Indeed, we found that membrane tension decreases as ES cells exit naïve pluripotency, and prohibiting ES cells from spreading inhibited both membrane tension reduction and naïve pluripotency exit. Importantly, decreasing membrane tension in constrained cells was sufficient to rescue the differentiation defect. These results suggest an important feedback between cell shape and cell surface mechanics during early differentiation of ES cells, but indicate that here it is cell surface mechanics that constitutes the primary mediator of cell fate transitions.

Our results also suggest a previously unknown synergy between essential pluripotency regulators β -catenin and FGF/ERK. This synergy demonstrates a clear feedback between cell signaling and surface mechanics: we show that β -catenin regulates membrane tension, which in turn gates downstream signaling activity by regulating endocytosis. We speculate that β -catenin regulates membrane tension by modulating RhoA activity via the Cadherin-Catenin complex which has been shown to regulate various Rho GTPases (Arnold et al., 2017). In this model, upon initiation of early differentiation, degradation of β -catenin by GSK3 leads to a drop in RhoA activity and subsequent decrease in ERM phosphorylation/membrane tension. Ultimately, our results suggest a role for β -catenin in maintaining naïve pluripotency by preserving high membrane tension, which would thus suppress endocytic FGF/ERK signaling in naïve cells.

Previous studies have pointed to correlations between mechanical changes and endocytosis, with links to cell fate (Pouille et al., 2009). Furthermore, osmotic changes, which among other effects

affect membrane tension, have been linked with endocytosis of receptors leading to inhibition of signaling pathways during transdifferentiation of muscle progenitors (Rauch et al., 2002). In contrast, our study demonstrates that in ES cells, FGF signaling is activated by increased endocytosis as a result of changes in cell surface mechanics. By unveiling a specific pathway activated as a result of a change in membrane tension, our study draws a direct link between cell mechanics, endocytic signaling, and fate choice.

Our findings point to plasma membrane tension as a central mediator of cell signaling. As the plasma membrane defines the boundary between the inside and outside of the cells it is an ideal cellular element to integrate environmental cues and mechanical changes into changes in cell signaling. Furthermore, we speculate that observed effects of substrate mechanics on stem cell fate regulation in other systems (Engler et al., 2006; Przybyla et al., 2016) might be in part due to resulting changes in membrane tension and downstream endocytosis rate. Going forward, it will be important to assess if and how the stiffness of the microenvironment can affect membrane tension. Given that many morphogenetic processes in development are accompanied by significant shape changes (Paluch and Heisenberg, 2009), it will also be interesting to further explore this connection *in vivo*. Taken together, our work unveils a mechanism directly connecting a specific change in cell mechanics to the activation of a key biochemical signaling pathway. The interplay between mechanics, membrane tension and endocytic signaling is likely to be an important regulator of cell fate in various developmental and pathological contexts.

Limitations of the study:

A limitation of our current study is the lack of quantitative 3D cell shape measurements. In our study we classified cells by shape using two categories: ‘round’ & ‘spread’. Quantitative cell shape measurement might allow us to identify an intermediary state between round and spread.

Also, as described in this study and others, differentiation is an asynchronous process. As such, bulk assays (Western Blots, RNAseq, etc) used in our investigation might lead to averaging out transient mixed populations.

Acknowledgements: We thank P. Attlesey and staff for animal husbandry, Carla Mulas for comments on the manuscript, Giorgio Scita for advice on endocytosis, Ortrud Warlick for help with setting up the optical tweezer, the MRC LMCB light microscopy facility for technical support, Anan Ragab and Mark Turmaine for their help with SEM, members of the Paluch lab (in particular Agathe Chaigne and Murielle Serres) and of the Chalut lab for technical help and advice at different stages of this project.

Funding: This work was supported by the European Union's Horizon 2020 research and innovation programme under the Marie Skłodowska-Curie grant agreement No 641639 (ITN Biopol, HdB and EKP), the Medical Research Council UK (MRC programme award MC_UU_12018/5, HdB and EKP), the Human Frontier Science Program (Young Investigator Grant RGY 66/2013 to EKP), the Leverhulme Trust (Prize in Biological Sciences to EKP), an ERC Consolidator Grant (*CellFateTech*, 772798, KC), a core support grant from the Wellcome Trust and Medical Research Council to the Wellcome Trust - Medical Research Council Cambridge Stem Cell Institute (KJC). KJC is a Royal Society University Research Fellow.

Author contributions: H.D.B., E.K.P., K.J.C. designed the research. E.K.P and K.J.C. supervised the research. H.D.B. carried out the bulk of experiments and data analysis. H.D.B., E.K.P., K.J.C. wrote the paper. A.S. carried out the gastruloids experiments and analysis. A.Y. carried the embryo experiments. C. L. carried out the RNAseq analysis. Funding Acquisition, E.K.P and K.J.C. P.J. built the optical tweezers setup. All authors discussed the results and manuscript.

Declaration of interests: Authors declare no competing interests.

Main figure titles and legends.

Figure 1: Membrane tension is reduced in ES cells during early differentiation.

A, Top: schematic of experimental setup to investigate exit from naïve pluripotency in ES cells; bottom: SEM images of ES and T48 cells. **B**, Representative single z-planes of T24 cells immunostained for Nanog and Otx2. **C**, Quantification of Nanog and Otx2 levels (from images as in B) in round (grey dots) and spread (red dots) T24 cells (N = 3). **D**, Schematic of membrane tension measurement using optical tweezers. **E**, left trap force (direct readout of membrane tension) during exit from naïve pluripotency of ES, T8, T16, T24 and T48 cells (mean \pm SD; 5 independent experiments). Data are colour coded based on cell shape (grey = round, orange = blebbing, red = spread). Right, same data as left panel but with all the data grouped by shape (e.g. all blebbing cells correspond to all the blebbing cells observed in T8, T16 and T24). **F**, Representative fluorescent Western Blot for pERM and His3 in ES cells and at various timepoint during exit from naïve pluripotency and corresponding quantification (N=4). *P* value was calculated using a two-way analysis of variance (ANOVA). For all panels, graphical data represents mean \pm SD. Unless otherwise indicated, for all panels p-values established by Welch's unpaired student t-test. Scale bars represent 10 μ m.

Figure 2: The decrease in membrane tension during early differentiation is induced by a β -catenin and RhoA mediated decrease in ERM phosphorylation.

A, Fluorescent Western Blot and associated quantification for pERM and GAPDH of WT and β -catenin knockout (KO) cells cultured in 2i+L (N=6). **B**, Trap force measurements of β -catenin KO ES cells and WT ES and T24 spread (S) cells (N=3). **C**, Schematic of the FRET sensor for RhoA activity. RBD stands for Rho binding domain. **D**, Representative images of the brightfield and FRET ratio of WT ES cells, T24 cells and β -catenin KO ES cells expressing the RhoA activation

FRET sensor. **E**, Quantification of the average FRET ratio (~RhoA activity) per cell. (N=3). **F**, Active RhoA pulldown assay. Top, representative fluorescent Western Blot for RhoA in WT ES, T24 and β -catenin KO cells after active RhoA pulldown. Bottom, quantification of active RhoA pulled down. (N=3). **G**, Top, representative fluorescent Western Blot for pERM and GAPDH in WT ES, iRhoA_CA ES & T24 cells. Note that WT 2i+L is same as in A (A and G are on the same gel). Bottom, corresponding quantification (N=4). **H**, Trap force measurement of WT ES, T24S, iRhoA_CA ES, T24 cells. (N=3). WT data in B and H are from figure 1E. Graphical data represents mean \pm SD. P-values established by Welch's unpaired student t-test and indicated in the figure. Scale bars represent 10 μ m.

Figure 3: Maintaining high membrane tension impairs early differentiation.

A, Representative images of WT (top) and iEZR_CA (bottom) ES and T48 cells. Scale bar, 50 μ m. **B**, Trap force, as a readout of membrane tension, for WT and iEZR_CA ES and T24 cells (N = 3; data for WT cells are same as Fig. 1H). **C**, Representative single z-planes of a mix of WT and iEZR_CA (positive for the EZR_CA_ires_mCherry) T24 cells immunostained for Otx2 and Nanog. Scale bar represents 10 μ m. **D**, Quantification of Nanog and Otx2 expression in WT and iEZR_CA T24 cells, normalised to WT mean levels (N=3). **E**, Left, schematic of clonogenicity assay used as a functional measure of naïve pluripotency. Right: quantification of the percentage of surviving replated cells in a clonogenicity assay using WT and iEZR_CA ES cells. Cells replated directly from 2i+L are used as a positive control (N=6). **F**, Heatmap of relative expression of main pluripotency genes and early post-implantation genes. The mean normalised log₂ counts for each timepoint in iEZR_CA cells is compared to mean normalised log₂ counts in WT cells. Averages were computed over 3 biological replicates. **G**, Principal component analysis from RNA-sequencing of iEZR_CA and wild type ESCs in 2i+LIF, and 24hr (T24) and 48hr (T48). Each marker represents an independent biological replicate (3 replicates per condition). The principal components (“PC”) were computed based on the normalised expression of highly variable genes (n = 4832 genes) (see methods). **H**, Schematic presentation of the gastruloid culture protocol: 300 mouse ES cells were transferred into low-attachment wells. CHIR99021 was introduced from 48 to 72 hours. Organoids were cultured for total 120 hours and images acquired at 72 h, 96 h and

120 h timepoints. **I**, Representative bright-field microscope images of gastruloids initiated from WT cells (left) iEZR_CA cells (right)

Figure 4: Membrane tension reduction, not cell spreading, is responsible for gating early differentiation.

A, Schematic of the micropatterning assay. Cells cannot adhere on PEG regions (blue) and can only adhere on the micropatterns. **B**, Representative single z-plane images of fixed ES and T24 cells cultured on small (top) and large (bottom) micropatterns and immunostained for Nanog. **C**, Quantification of Nanog expression in ES and T24 cells cultured on large (unconstrained, control) and small (constrained) micropatterns (here, p-values were calculated using Mann-Whitney U test, N = 4). **D**, Membrane tension measurements in ES cells and T24 cells either grown on micropatterns (small – constrained or large – unconstrained), or cultured in an open gelatin-coated dish (ES and T48). Data for cells on gelatine are from Figure 2B. (N=2). **E**, Similar quantifications as in (C) but for cells transfected with triple siRNA against ERM or with SCR as control (Mann-Whitney U test was used to calculate p-value, N = 4). **F**, Representative images of ES and T24 cells cultured on laminin and E-Cadherin. **G**, Trap force measurements in ES cells and T24 cells cultured on either gelatine, laminin or E-Cadherin. Data for cells cultured on gelatine are the same as Figure 2B. (N=3). Graphical data represents mean \pm SD. Unless otherwise specified, p-values calculated using Welch's unpaired student t-test. Scale bars represent 10 μ m.

Figure 5: Endocytosis regulates early differentiation.

A, Schematic of endocytosis quantification using a fluid uptake assay with pH sensitive fluorescent dextran. **B, C**, Sum z-projection images of representative ES and T24 cells in assay described in A, B, and corresponding quantification (C; error bars are 95% Confidence Intervals; N=3). **D**, Left: schematic of endocytosis quantification assay with the use of drug treatment against endocytosis. Right, quantification of fluid phase uptake in ES, T24 cells treated with either DMSO (control), Chlorpromazine hydrochloride (10 μ M), PitStop2 (25 μ M) or Dynasore (10 μ M). **E**, Representative images of immunofluorescence against Nanog and Otx2 of a single z-plane of T24 cells treated with either DMSO (control), Chlorpromazine hydrochloride (10 μ M), PitStop2 (25 μ M) or Dynasore (10 μ M). **F,G**, Quantification of Nanog and Otx2 expression in cells treated with drugs

to inhibit endocytosis, normalised to control (DMSO) mean levels (N=3). **H, I**, Sum z-projection images of representative WT ES cells, iEZR_CA-ES cells and iEZR_CA-ES cells transfected with Rab5a in assay described in A, and associated quantifications. Error bars: 95% Confidence Intervals (N=3). **J, K**, Single z-plane images of representative mixed populations of WT and iEZR_CA (positive in the mCherry channel) T24 cells, transfected with Rab5a and immunostained for Nanog and corresponding quantifications (N=3). Non transfected iEZR_CA data are from Fig. 2D. Graphical data represents mean \pm SD. P-values calculated using Welch's unpaired student t-test. Scale bars represent 10 μ m.

Figure 6: Membrane tension mediated endocytosis promotes ERK activation during early differentiation.

A, Fluorescent Western blot for ERK, pERK and Histone3 in ES cells at different timepoints during exit from naïve pluripotency (see Extended data Fig. 9 for uncropped Western blots). **B**, Time-course of the ratio of pERK levels (normalised to corresponding Histone 3 levels) in WT and iEZR_CA cells during exit from naïve pluripotency (N=6). **C**, Representative single z-plane image of WT, iEZR_CA and iEZR_CA T24 treated with 3 μ M of BI-D1870, an RSK-inhibitor (resulting in ERK activation) immunostained for Nanog and Otx2. **D**, Quantification of Nanog and Otx2 expression in WT, iEZR_CA, iEZR_CA+BI-D1870 T24 cells, normalised to WT mean levels (N=3). **E**, Schematic of the FRET ERK sensor used to measure ERK activation at early endosomes (Palamidessi et al., 2019). **F**, Left, Time-lapse of representative cell expressing the FRET ERK sensor and exiting pluripotency at 6 h (top, the cell is still round) and 18h20 (bottom, the cell is spread). Right, Timecourse of the FRET ratio for the cell shown at left. **G**, Quantification of the FRET ratio in ES cells exiting naïve pluripotency, time is normalised to the time of spreading (means \pm SEM, n=10, N=3). Inset: FRET ratio for round and spread cells in the same dataset. **H**, Mean FRET ratio for fixed ES and T24 cells in WT and iEZR_CA transfected or not with Rab5a (N=3). **I**, Schematic of the proposed mechanism for how membrane tension regulates signalling during exit from naïve pluripotency. Graphical data represents mean \pm SD. P-values calculated using Welch's unpaired student t-test (unless specified otherwise) and indicated in the figure. Scale bars represent 10 μ m.

STAR methods

KEY RESOURCES TABLE

| REAGENT or RESOURCE | SOURCE | IDENTIFIER |
|--|--------------------------|-----------------|
| Antibodies | | |
| phospho ERK | Cell Signaling | 4370 S |
| ERK | Cell Signaling | 9107 S |
| Nanog | eBioscience | eBioMLC-51 |
| Otx2 | R&D Systems | AF1979 |
| ERM | Cell Signaling | 3142S |
| Phospho ERM | Cell Signaling | 3149S |
| GAPDH | Abcam | ab8245 |
| His3 | Abcam | Ab1701 |
| Fgfr1 | Abcam | ab10646 |
| Chemicals, Peptides, and Recombinant Proteins | | |
| B27 | Life technologies | Cat#12587010 |
| CHIRON | Cambridge Bioscience | Cat#CAY13122 |
| PD 0325901 | Sigma-Aldrich | Cat#PZ0162 |
| LIF | Merck Millipore | Cat# ESG1107 |
| Insulin zinc | Sigma-Aldrich | Cat#I9278 |
| Apotransferrin | Sigma-Aldrich | Cat# T1147 |
| Laminin | Sigma-Aldrich | Cat#11243217001 |
| Lipofectamin TM RNAimax | ThermoFischer Scientific | Cat# 13778075 |
| Accutase | Sigma-Aldrich | Cat#A6964 |
| DMEM/F-12, 1:1 mixture | Sigma-Aldrich | Cat#D6421-6 |
| Neurobasal medium | Life technologies | Cat#21103-049 |
| Lipofectamine [®] 2000 Transfection Reagent | Life technologies | Cat#11668-027 |
| Hoechst | ThermoFischer | Cat#34580 |
| DAPI | Sigma-Aldrich | Cat#9542 |
| Dynasore | Sigma-Aldrich | Cat#D7693 |
| NSC 23766 | Tocris | Cat#2161 |
| Methyl-B-Cyclodextrin | Sigma-Aldrich | Cat#C4555 |
| BI-D1870 | VWR | Cat#501437-28-1 |
| PitStop2 | Abcam | Cat#Ab120687 |
| Chlorpromazine hydrochloride | Sigma-Aldrich | Cat#D22914 |
| Dextran, Alexa Fluor TM 647, 10,000 MW | ThermoFischer | Cat#D22914 |
| pHrodo TM Red Dextran, 10,000 MW | ThermoFischer | Cat#P10361 |
| Critical Commercial Assays | | |

| | | |
|--|---|-----------------------|
| Active RhoA pulldown assay | Cytoskeleton Inc | Cat#BK036 |
| Deposited Data | | |
| RNA seq: GEO accession number GEO: GSE159433 | https://www.ncbi.nlm.nih.gov/geo/query/acc.cgi?acc=GSE159433 | N/A |
| Experimental Models: Cell Lines | | |
| Mouse embryonic stem cells: E14 | Chalut lab (Cambridge Stem cell Institute, Cambridge, UK) | N/A |
| Mouse embryonic stem cells: EZR_CA | Chalut lab (Cambridge Stem cell Institute, Cambridge, UK) | Yanagida et al., 2020 |
| Mouse embryonic stem cells: RhoA_CA | Chalut lab (Cambridge Stem cell Institute, Cambridge, UK) | Yanagida et al., 2020 |
| Mouse embryonic stem cells: H2B-mCherry | Nichol's lab (Cambridge Stem cell Institute, Cambridge, UK) | N/A |
| Mouse embryonic stem cells: LifeAct GFP | Ian Rosewell (Francis Crick Institute, London, UK) | Riedl et al., 2010 |
| Mouse embryonic stem cells: Beta-Catenin KO | Smith's lab (Cambridge Stem cell Institute, Cambridge, UK) | Wray et al., 2011 |
| Oligonucleotides | | |
| SMARTpool: ON-TARGETplus Ezr siRNA | Dharmacon | L-046568-01 |
| SMARTpool: ON-TARGETplus Rdx siRNA | Dharmacon | L-047230-01 |
| SMARTpool: ON-TARGETplus Msn siRNA | Dharmacon | L-044428-01 |
| SMARTpool: ON-TARGETplus MYO1C siRNA | Dharmacon | L-015121-00 |
| SMARTpool: ON-TARGETplus Myo1b siRNA | Dharmacon | L-045103-01 |
| siGENOME Non-Targeting Control siRNA #3 | Dharmacon | D-001210-03 |
| siGENOME Non-Targeting Control siRNA #5 | Dharmacon | D-001210-05 |
| siGENOME Non-Targeting Control siRNA #2 | Dharmacon | D-001210-02 |
| Software and Algorithms | | |
| Fiji | Schindelin, J.et al. (2012). | N/A |
| Prism 8 | Graphpad software, Inc | N/A |

Resource availability

Lead Contact: Further information and requests for resources and reagents should be directed to and will be fulfilled by the Lead Contact, Kevin J Chalut, kc370@cam.ac.uk

Materials Availability: This study did not generate new unique reagents

Data and Code Availability: The accession number for the RNA sequencing data reported in this paper is GEO: GSE159433 (accessible through:

<https://www.ncbi.nlm.nih.gov/geo/query/acc.cgi?acc=GSE159433>)

EXPERIMENTAL MODEL AND SUBJECT DETAILS

Cell lines

ES-E14TG2a (referred as WT) directly derived from mouse embryos were a kind gift from the Austin Smith's laboratory (Cambridge Stem Cell Institute). The LifeAct GFP cell line is from (Riedl et al., 2010). These cells have been generated and kindly given to us by Ian Rosewell (Francis Crick Institute, under Holger Gerhardt's project license). Dox-inducible IRES mCherry Ezrin_CA & RhoA_CA ES (Yanagida et al., 2020) cells were kindly given to us by Ayaka Yanagida from the Chalut and Nichols's lab. The EZR_CA was engineered using a PiggyBac system with E14 ES cells. The H2B-mCherry cells were kindly given to us by Tim Lohoff from the Nichol and Reik's lab. The β -Catenin Knockout cell line was kindly given to us by the lab of Austin Smith and has been described in (Wray et al., 2011).

Mice and mice embryos

Mice used were intercrosses of CD1 (Charles River). All embryos used in this study were obtained from natural mating. Embryo staging was based on the assumption that, on average, mating occurred at midnight so that at midday, the embryos were assigned E0.5. Embryos were flushed at the relevant stages from oviduct (eight-cell stage embryos) using flushing and holding a medium (M2, Sigma). The sex of embryos and the ages of mice using mating were not concerned in this study. This research has been regulated under the Animals (Scientific Procedures) Act 1986 Amendment Regulations 2012 following ethical review by the University of Cambridge Animal Welfare and Ethical Review Body (AWERB). Use of animals in this project was approved by the ethical review committee for the University of Cambridge, and relevant Home Office licences (Project licence No. P76777883) are in place.

Methods details

Cell culture, transfections and exit from naïve pluripotency

Mouse embryonic stem cells were cultured on Falcon flasks coated with 0.1% gelatine. On occasion, laminin (Sigma-Aldrich #11243217001) coated dishes were used instead of gelatine. ES cells used were E14TG2a. Cells were cultured in N2B27+2i+LIF (2i+L) (Mulas et al., 2019) at 37°C with 7% CO₂. Cells were passaged every other day using Accutase (Sigma-Aldrich, #A6964) and regularly tested for mycoplasma. Culture medium was changed every 24h. The culture medium was made using DMEM/F-12, 1:1 mixture (Sigma-Aldrich, #D6421-6), Neurobasal medium (Life technologies #21103-049), 2.2 mM L-Glutamin, B27 (Life technologies #12587010), 3 µM Chiron (Cambridge Bioscience #CAY13122), 1 µM PD0325901 (Sigma-Aldrich #PZ0162), 20 ng/ml of LIF (Merck Millipore # ESG1107), 50 mM β-Mercapto-ethanol, 12.5 ng.mL⁻¹ Insulin zinc (Sigma-Aldrich #I9278) and home-made N2. The 200 X home-made N2 was made using 0.791 mg.mL⁻¹ Apotransferrin (Sigma-Aldrich #T1147), 1.688 mg.mL⁻¹ Putrescine (Sigma-Aldrich #P5780), 3 µM Sodium Selenite (Sigma-Aldrich #S5261), 2.08 µg.mL⁻¹ Progesterone (Sigma-Aldrich #P8783), 8.8% BSA. Exit from naïve pluripotency was triggered by passaging ~500 000 cells and seeding them in N2B27 only (N2B27) on T25 gelatine coated flasks.

Transfections of plasmids were performed using 5 µg of plasmid and 3.5 µL of Lipofectamine 2000 (ThermoFischer Scientific #11668019), incubated in 250 µL OptiMEM for 5 minutes, then mixed and incubated at room temperature for 30 minutes, and added to cells passaged onto Ibidi dishes with polymer coverslip bottom for observations (IBIDI Scientific, 81156).

Due to the lack of fluorescent tag, transfection efficiency of Rab5a was assessed by performing immunofluorescence against Rab5a of un-transfected and transfected cells. Average fluorescence level was determined in transfected and untransfected cells by measuring average fluorescence intensity using Fiji (Schindelin et al., 2012). Cells with an average fluorescence higher than 20% of the average of untransfected cells were counted as being positively transfected. Using this method, we estimate Rab5a transfection efficiency to be ~72%. siRNA transfections were performed using 30 µM of siRNA and 5 µL of Lipofectamine RNAiMAX (ThermoFischer Scientific #13778075) incubated in 250 µL OptiMEM for 5 minutes, then mixed and incubated at room temperature for 30 minutes and added to cells passaged onto micropatterns.

Tether pulling and trap force measurements

Trap force measurements were performed using a home-built optical tweezer using a 4W 1064 nm Laser Quantum Ventus with a 100x oil immersion objective (NA 1.30, CFI Plan Fluor DLL, Nikon) on an inverted microscope (Nikon Eclipse TE2000-U) equipped with a motorized stage (PRIOR Proscan). The optical tweezer was calibrated following (Lieber et al., 2013). Measurements were performed using concanavalin-

A coated (50 $\mu\text{g/ml}$) carboxyl latex beads (1.9 μm diameter, Thermo Fisher C37278). Beads were incubated on a shaker with concanavalin-A for one hour prior to the experiment. Bead position was recorded every 90 milliseconds in bright field prior and during tether formation. The trap force was calculated based on the calibration of the trap and the bead position using a home-made Fiji (Schindelin et al., 2012) plugin (HDB) (typical values for the trap stiffness were $k \sim 0.130$ pN/nm.)

RNA extraction and qPCR

Cells were seeded in 6 well dishes in different conditions (N2B27 or 2i+L) and cultured for different periods of time, as indicated. RNA was extracted using a Qiagen (205310) kit. Extracted RNA cDNA was generated from the RNA according to kit's instructions (Thermo Fischer Scientific #4368814). For the RT-qPCR, pre-designed primers (see table of primers used), and the SYBR Green Master Mix (Qiagen; 204141) were combined according to the kit's instructions. qPCR was performed on Bio-Rad CFX qPCR.

Western blots

Cells were plated into 6-well plates in different conditions (with or without 2i+L), as indicated. Proteins were extracted on ice using Laemmli buffer (Bio-Rad #1610747). Samples were put at 95° C for 5 min and then sonicated on ice. Isolated whole protein content was measured using the Thermo Scientific Pierce 660nm Protein assay (#22660) using a BSA gradient kit (Bio-Rad; 500-0206) and 20 μg of protein extract was loaded onto either NuPAGE 4-12% Bis-Tris protein gels (Thermo Fischer Scientific #NP0321BOX) or Novex WedgeWell 14% Tris-Glycine Mini Gels (Thermo Fischer Scientific #XP00140BOX) depending on the size of the protein of interest. Gels were run at 125 V for 2 h. Proteins were transferred for 70 minutes at 70 V to a nitrocellulose membrane (Thermo Fischer Scientific #88024). Membranes were blocked for 90 min using Odyssey blocking buffer (Licor #927-50003). Primary antibodies were added at the proper dilution (see table of antibodies) in either TBS-T + 5% milk or 5% BSA and incubated overnight at 4 degrees. Membranes were washed three times for 15 min in TBS with TWEEN. Infrared species-appropriate secondary antibodies were then added (see table of antibodies) for one hour. Membranes were washed three times with PBS-T for 15 min and imaged on the Licor Odyssey scanner. Bands were quantified using LI-COR Biosciences Image Studio Lite.

Immunofluorescence

Cells were fixed in IBIDI dishes (IBIDI Scientific, 81156) with 4% formaldehyde. Cells were permeabilized during 10 min in PBS+0.1% Triton-X. Blocking was then done using with 2% FBS 2% BSA in PBS with 0.1% Triton for 45 min. Cells were then incubated for 1h30min with the primary antibody diluted at the appropriate concentration in the same buffer as used for blocking. Cells were then washed 3

times 5 min with PBS+0.1% Triton. Secondary antibodies were added for 1 h diluted at 1:800 in the same buffer as used for blocking and primary antibody incubation. Cells were washed with PBS + 0.1% Triton 3 times for 5 min. Finally, cells were incubated for 5 min with PBS+DAPI before a final rinse in PBS.

RNA sequencing, data processing, differential expression analysis and gene ontology analysis

Library preparation was done by in-house facility us NEBNext® Multiplex Oligos for Illumina. Paired-end sequencing was performed using the Novaseq sequencing platform, yielding 517 million reads (single-lane). Reads were trimmed and adapters removed using FastQC and TrimGalore (Babraham Bioinformatics). Mouse genome build GRCm38/mm10 was used to align reads with GSNAP version 2015-09-29 (Wu and Nacu, 2010). Genes were annotated using Ensembl release 81 (Cunningham et al., 2015) and read counts were quantified using HTSeq (Anders et al., 2015). Differential expression analysis was computed using DESeq2 (Love et al., 2014) a design containing an interaction term (TimePoint:CellType). For gene ontology analysis, the significant interaction terms at 24hrs and 48hrs were selected (i.e. differently regulated between iEZR_CA cells and wild type cell during exit from naïve pluripotency), using thresholds of base mean >5 and an absolute log₂ fold change >1. DAVID 6.8 (Huang et al., 2009a, 2009b) was used to compute the statistical enrichment of Gene Ontology terms. For each category (KEGG Pathway and Cellular Component), the list of enriched terms was filtered using Benjamini-Hochberg false-discovery rate correction ($p_{adj} < 0.1$). Additionally, only terms with fold enrichment ≥ 2 and at least 1% of annotated genes regulated were selected. The top 5 (ordered on increasing adjusted p value) are plotted for each of the four functional annotations category.

Highly variable genes were determined by averaging, for each gene, the intra-group variance (3 replicates per group, 6 experimental groups). The intra-group (or technical) variance was then compared to the distribution of variance computed over 3 randomly selected samples (inter-group variance). Highly variable genes were those for which the technical variance was significantly lower than the inter-group variance.

Micropatterning

Glass coverslips (Marienfeld GmbH) were sonicated in 1 M of HCl for 5-15 minutes, washed and plasma-treated for 30 seconds for glass passivation. Then 0.1 mg/mL of PLL-g-PEG (PLL(20)-g[3.5]-PEG(2)/Atto663 from SuSoS) solution was added to the coverslips for 30 min at room temperature. Chrome MASK from Delta Mask was used. The mask was illuminated with UV light for 5 min on the chrome side, then the PEG-coverslips were added on the chrome side and illuminated for 6 min to burn the PEG in the

shape of the desired pattern (circles in our case). Coverslips were then dried and stored. Coverslips were rehydrated before use.

For immunofluorescence assays, we seeded the cells onto the patterns (coated with laminin, see above for details) in 2i+L at a density allowing for the formation of small colonies, occupying the whole available space on the small circles while still having free space on the bigger circles. Cells were then washed three times in PBS and placed in N2B27 only without 2i+L. After 24h in N2B27, cells were fixed and immunostained.

Generation of chimaeras

ES cells (five to eight cells per embryo) were injected into eight-cells embryos via a laser-generated perforation in the zona pellucida using XYClone (Hamilton Thorne Biosciences). Injected embryos were cultured in N2B27 with or without 1µg/ml Dox for two-days for eight-cells injection or one-day for blastocyst injection, an equivalent of E4.5 blastocysts at 37°C and 5% CO₂.

Isolation of ICMs from embryos, and *in vitro* culture

Embryo and cell manipulations were carried out under a dissecting microscope (Leica Microsystems). The zona pellucida was removed using acid Tyrode's solution (Sigma) at E4.0. E4.5 blastocysts were subjected to immunosurgery as previously described (Solter and Knowles, 1975). In brief, blastocysts were incubated for 45-60 minutes in a 1:5 dilution of anti-mouse rabbit serum (Sigma) in N2B27, washed in N2B27 and further incubated for 30-60 minutes in a 1:5 dilution of rat serum (in-house) in N2B27 for the complement reaction. The ICM was subsequently cleaned from residual trophectoderm with a narrowly fitting glass pipette. Isolated ICMs were culture in N2B27 at 37°C and 5% CO₂ with or without 1µg/ml Dox an equivalent to E5.5 in which PrE lineage cells surround the matured EPI.

RhoA pulldown assay

RhoA pulldown assay was performed using the Cytoskeleton Inc pull down kit (#BK036) and carefully following the provided instructions. In a nutshell, the assay is using beads coated with the Rho binding domain of Rhotekin, a rho effector protein which bind specifically to the GTP-bound RhoA. His tagged RhoA protein and GTPγS were used as controls.

Immunofluorescence staining

Embryos or one-day cultured isolate ICMs were fixed with 4% paraformaldehyde (PFA; Thermo Fisher Scientific) in Phosphate buffered saline (PBS; Sigma) at room temperature for 15 minutes. Then, the

samples were rinsed in PBS containing 3 mg/ml polyvinylpyrrolidone (PBS/PVP; Sigma), permeabilised with PBS/PVP containing 0.25% Triton X-100 for 30 minutes. Blocking was performed with a buffer comprising PBS containing 0.1% bovine serum albumin (BSA; Sigma), 0.01% Tween20 (Sigma) and 2% donkey serum at 4°C for 2-3 hours. Primary antibodies (See table of antibodies below) were diluted in blocking buffer, and samples were incubated in the appropriate antibody solution at 4°C overnight. They were rinsed three times in blocking buffer for 15 minutes ~ each. Secondary antibodies were diluted in blocking buffer with 500 ng/ml 4',6-diamidino-2-phenylindole (DAPI; Invitrogen) and samples were incubated in the appropriate antibody solution at room temperature for one hour in the dark. They were rinsed three times in blocking buffer for 15 minutes ~ each. Whole staining process was performed on a microwell mini Tray (Nunc). Embryos or cultured isolated ICMs were put in a small drop of blocking buffer on poly-D-lysine (Sigma) coated glass-bottom dishes (MatTek) covered with mineral oil (Sigma), and their images were acquired using a Leica TCS SP5 confocal microscope.

Gastruloid culture

Gastruloids produced as described before (Baillie-Johnson et al., 2015). Briefly, mouse ES cells were detached from gelatin-coated vessels using accutase for 4 min (Sigma, A6964). The iEZR_CA ES cells were cultured with doxycycline for 24 h or 48 h before aggregation and during the following protocol. Detached cells were then washed once with warm N2B27 and twice with warm PBS (Sigma, D8537). In between the washes, the cells were pelleted for 3 min at 170 x g. Subsequently, the cells were resuspended to fresh N2B27 and the number of cells counted using an automated cell counter (Merck, Scepter 2.0, PHCC20040). The cell suspension was diluted so that 40 ul of suspension had 300 cells. 40 ul of suspension was then transferred to low attachment 96 well round-bottomed plates (Sigma, M3562) for 48 h of aggregation. Next, 150 ul of fresh N2B27 medium with 3 uM CHRI99021 (Cambridge Bioscience, CAY13122) was pipetted to the wells for 24 hours. After which 150 ul of fresh N2B27 medium was changed to the wells daily until 120 hours.

Gastruloid morphometric analysis

WT and iEZR_CA organoids were imaged using a cell culture microscope (Olympus, CKX53SF) and 10x air objective (Olympus, NA 0.25) mounted with a digital camera (Canon, EOS 250D). The resulting images were analysed with ImageJ Fiji distribution (Schindelin et al., 2012). Briefly, the images were opened as an image stack and converted to 8-bit grayscale images. Next, the grayscale images were thresholded manually to best segment the organoid outlines. The resulted binary masks were then measured using Fiji build in analyse particles function. “Feret’s diameter” and “shape descriptors” were recorded and analysed.

Fluid phase uptake assay

Cells were seeded on IBIDI dishes (IBIDI Scientific, 81156) a few hours before imaging. Cells were then incubated for 10 min in N2B27 or 2i+L with 10 µg of either pH-Rhodo Dextran (pHrodo™ Red Dextran, 10,000 MW, for Endocytosis, Thermofischer Scientific) or Alexa Fluor Dextran (Dextran, Alexa Fluor™ 647; 10,000 MW, Thermofischer Scientific)(Rappaport et al., 2016). Cells were then rinsed immediately prior to imaging. Each dish was imaged for 30 min.

For quantifications with either pH Rhodo or Regular Dextran, total intensity inside the cell was measured with Fiji by using a sum z projection. The signal was corrected by taking a ROI of the background of a similar size as of the measured cells. The background signal was then subtracted from the signal from cell. Only single cells or groups of cells with clear boundaries were quantified. CellMask Deep Red (Invitrogen # C10046) was used to identify individual cell boundaries. Experiments were always performed side by side with cells in 2i+LIF as control. Data are normalised to cells in 2i+L.

FRET analysis

Imaging was performed on an inverted confocal microscope (Olympus FV1200), at 37°C with 5% CO₂ for live imaging, taking z-stacks 10µm in total height with a 1µm step using a 63x objective. For FRET quantifications, we used a home-written (HDB) custom Macro in Fiji (Schindelin et al., 2012) FRET and donor channel signals were corrected for background.

For the FRET sensor for RhoA activation (Pertz et al., 2006), a sum-projection was performed before FRET quantification. We then measured average ratio in each cell by using three circular ROIs (of 1µm diameter) in the region of positive FRET ratio (thus at the cell cytoplasm or cortex and not in the nucleus for example). We then averaged the obtained data for each cell.

For the FRET sensor for ERK activation in the endosome, vesicles were semi-automatically identified and average fluorescence was quantified in each vesicle across all the channels. Small Z maximum projections (over 3 z slices of 1µm) were quantified in order to ensure capture entire endocytotic vesicles. We then calculated the ratio of values obtained in donor and FRET channels to obtain FRET ratio following (Deathridge et al., 2019; Palamidessi et al., 2019) methods.

Clonogenicity assay

To test for speed and efficiency of exit from pluripotency, replating assays were performed. For each experimental condition, ~400 000 cells were plated onto 6-well dishes coated with 0.1% gelatin, in N2B27 to induce exit from naïve pluripotency. After 48h in N2B27, the cells were resuspended and counted. A specific number of cells (typically 400) was then replated in N2B27+2i+L onto a 12-well plate. After 4 days, the number of colonies was manually counted; as only naïve cells survive in 2i+L, this assay quantifies

the efficiency of pluripotency exit. As a positive control, cells cultured in 2i+L were replated in 2i+L. Occasionally replated cells were tested for naïve pluripotency using a Blue-colour AP staining kit to add another control that replated cells were indeed naïve pluripotent (Cambridge Bioscience #AP100B-1).

Scanning Electron Microscopy

Samples were fixed with glutaraldehyde 1%. Preparation for scanning electron microscopy was performed as in (Chugh et al., 2017) without membrane extraction. Jeol 7401 - high resolution Field Emission Scanning Electron Microscope was used for imaging.

Plasmids

Rab5a and FRET plasmids were provided by Giorgio Scita's lab (Palamidessi et al., 2019)

Ezr_GFP and EZR_CA_GFP were provided by Guillaume Charras (Gautreau et al., 2000)

FRET RhoA sensor was obtained from Adgene (#12150) and is characterised in (Pertz et al., 2006)

Quantification and statistical analysis

Live imaging was performed on an inverted confocal microscope (Olympus FV1200), at 37°C with 5% CO₂, taking z-stacks 10µm in total height with a 1µm step using a 63x objective and using low laser power. Fix imaging was performed on an inverted confocal microscope (Leica TCS SP5) taking z-stacks 20µm in total height with a 1µm step using a 63x objective. All image analysis were performed using Fiji (Schindelin et al., 2012).

To measure Nanog and Otx2 levels, we used DAPI to locate the cell nuclei, identified the nuclei mid plane and make a ROI of the nucleus. We then used this ROI to measure average Nanog or Otx2 intensity per nucleus, thus controlling for cell/nuclear size in measuring transcription factor expression.

For pERM measurements by IF, we used a sum-projection. We then identified ROIs in the cell (using the cortical actin identified via the phalloidin channel (Alexa Fluor 568 Phalloidin (ThermoFischer Scientific # A12380)) as boundary for the ROI) and measured the integrated signal (the mean intensity signal*number of pixels in the selection) to compensate for differences in cell size. Additionally, we corrected the measured values by subtracting background using the same ROI as for the cell but in a region with no cell present. Data were normalised to round cells. signal was used to determine cell boundaries and to classify cells according to shape based on visual inspection.

For Fgfr1 quantifications, average fluorescence was measured in each cell using CellMask Deep Red (Invitrogen # C10046) as a marker to locate individual cells. Average intensity was then manually measured in the midplane of the cells by taking a ROI following the cell boundary.

For #blebs in Supp Figure 1, the number of blebs was manually counted at every time point (every 20 minutes) across a z-stack using LifeAct and brightfield as guides to identify individual blebs (note that only actin filled blebs could be observed with this method).

For all statistical analysis, PRISM 7 (Graphpad software, Inc) was used. Statistical details can be found in the legend of each figure. D'agostino and pearson test was used to test for normality. N represents number of independent biological replicates. Pooled independent experiments are used in dot plots.

Figure S1. Membrane to cortex attachment and membrane tension are decreased during early differentiation. Related to Figure 1.

Figure S2. pERM activity and membrane tension during early differentiation are regulated by β -catenin and RhoA. Related to Figure 2.

Figure S3. Increasing membrane tension inhibits early differentiation. Related to Figure 3.

Figure S4. Maintaining a high membrane tension impairs exit from naïve pluripotency independently of cell shape. Related to Figure 4.

Figure S5. Endocytosis levels regulate exit from naïve pluripotency. Related to Figure 5.

Figure S6. ERK signalling and FGFR1 expression in exit from naïve pluripotency. Related to Figure 6.

Table S1. RNAseq dataset of WT & iEZR_CA ES, T24 & T48 cells, Related to Figure 3 & 6.

Movie S1. Time-lapse (confocal) of LifeAct ES cells exiting naïve pluripotency. Movie starts at 6 h after medium change to N2B27. One frame is shown every 20 min. Related to Figure 1.

Movie S2. Time-lapse (brightfield) of a ES cell where a membrane tube is pulled with an optical tweezer. One frame is shown every second. A red target has been added to visualize the center of the laser trap. Related to Figure 1.

Movie S3. Time-lapse (confocal) of ES cells exiting naïve pluripotency and transfected with FRET sensor for ERK activity. Movie starts after 6 h in N2B27. One frame is shown every 20 minutes. A single z-slice is shown. Related to Figure 6.

References and Notes:

- Anders, S., Pyl, P.T., and Huber, W. (2015). HTSeq--a Python framework to work with high-throughput sequencing data. *Bioinformatics* *31*, 166–169.
- Arnold, T.R., Stephenson, R.E., and Miller, A.L. (2017). Rho GTPases and actomyosin: Partners in regulating epithelial cell-cell junction structure and function. *Experimental Cell Research* *358*, 20–30.
- Avior, Y., Sagi, I., and Benvenisty, N. (2016). Pluripotent stem cells in disease modelling and drug discovery. *Nat. Rev. Mol. Cell Biol.* *17*, 170–182.
- Baillie-Johnson, P., van den Brink, S.C., Balayo, T., Turner, D.A., and Martinez Arias, A. (2015). Generation of Aggregates of Mouse Embryonic Stem Cells that Show Symmetry Breaking, Polarization and Emergent Collective Behaviour In Vitro. *J Vis Exp*.
- Bellas, E., and Chen, C.S. (2014). Forms, forces, and stem cell fate. *Current Opinion in Cell Biology* *31*, 92–97.
- Bergert, M., Lembo, S., Milovanović, D., Börmel, M., Neveu, P., and Diz-Muñoz, A. (2020). Cell surface mechanics gate stem cell differentiation. *Cell Stem Cell*, this issue.
- Biswas, A., Kashyap, P., Datta, S., Sengupta, T., and Sinha, B. (2018). Cholesterol depletion by M β CD enhances membrane tension, its heterogeneity and affects cellular integrity. *BioRxiv* 264036.
- Boroviak, T., Loos, R., Lombard, P., Okahara, J., Behr, R., Sasaki, E., Nichols, J., Smith, A., and Bertone, P. (2015). Lineage-Specific Profiling Delineates the Emergence and Progression of Naive Pluripotency in Mammalian Embryogenesis. *Developmental Cell* *35*, 366–382.
- Chalut, K.J., and Paluch, E.K. (2016). The Actin Cortex: A Bridge between Cell Shape and Function. *Developmental Cell* *38*, 571–573.
- Charras, G., and Paluch, E. (2008). Blebs lead the way: how to migrate without lamellipodia. *Nature Reviews Molecular Cell Biology* *9*, 730–736.
- Chen, G., Schell, J.P., Benitez, J.A., Petropoulos, S., Yilmaz, M., Reinius, B., Alekseenko, Z., Shi, L., Hedlund, E., Lanner, F., et al. (2016). Single-cell analyses of X Chromosome inactivation dynamics and pluripotency during differentiation. *Genome Res.* *26*, 1342–1354.
- Chugh, P., Clark, A.G., Smith, M.B., Cassani, D.A.D., Dierkes, K., Ragab, A., Roux, P.P., Charras, G., Salbreux, G., and Paluch, E.K. (2017). Actin cortex architecture regulates cell surface tension. *Nat. Cell Biol.* *19*, 689–697.
- Clark, A.G., Wartlick, O., Salbreux, G., and Paluch, E.K. (2014). Stresses at the Cell Surface during Animal Cell Morphogenesis. *Current Biology* *24*, R484–R494.

- Connelly, J.T., Gautrot, J.E., Trappmann, B., Tan, D.W.-M., Donati, G., Huck, W.T.S., and Watt, F.M. (2010). Actin and serum response factor transduce physical cues from the microenvironment to regulate epidermal stem cell fate decisions. *Nat. Cell Biol.* *12*, 711–718.
- Cunningham, F., Amode, M.R., Barrell, D., Beal, K., Billis, K., Brent, S., Carvalho-Silva, D., Clapham, P., Coates, G., Fitzgerald, S., et al. (2015). Ensembl 2015. *Nucleic Acids Res* *43*, D662–D669.
- Dai, J., and Sheetz, M.P. (1995). Regulation of Endocytosis, Exocytosis, and Shape by Membrane Tension. *Cold Spring Harb Symp Quant Biol* *60*, 567–571.
- Deathridge, J., Antolović, V., Parsons, M., and Chubb, J.R. (2019). Live imaging of ERK signaling dynamics in differentiating mouse embryonic stem cells. *Development dev.* 172940.
- Diz-Muñoz, A., Krieg, M., Bergert, M., Ibarlucea-Benitez, I., Muller, D.J., Paluch, E., and Heisenberg, C.-P. (2010). Control of Directed Cell Migration In Vivo by Membrane-to-Cortex Attachment. *PLOS Biology* *8*, e1000544.
- Diz-Muñoz, A., Fletcher, D.A., and Weiner, O.D. (2013). Use the force: membrane tension as an organizer of cell shape and motility. *Trends in Cell Biology* *23*, 47–53.
- Dutta, D., and Donaldson, J.G. (2012). Search for inhibitors of endocytosis. *Cell Logist* *2*, 203–208.
- Engler, A.J., Sen, S., Sweeney, H.L., and Discher, D.E. (2006). Matrix Elasticity Directs Stem Cell Lineage Specification. *Cell* *126*, 677–689.
- Evans, M.J., and Kaufman, M.H. (1981). Establishment in culture of pluripotential cells from mouse embryos. *Nature* *292*, 154–156.
- Gautreau, A., Louvard, D., and Arpin, M. (2000). Morphogenic effects of ezrin require a phosphorylation-induced transition from oligomers to monomers at the plasma membrane. *J. Cell Biol.* *150*, 193–203.
- Gudipaty, S.A., Lindblom, J., Loftus, P.D., Redd, M.J., Edes, K., Davey, C.F., Krishnegowda, V., and Rosenblatt, J. (2017). Mechanical stretch triggers rapid epithelial cell division through Piezo1. *Nature* *543*, 118–121.
- Guilak, F., Cohen, D.M., Estes, B.T., Gimble, J.M., Liedtke, W., and Chen, C.S. (2009). Control of stem cell fate by physical interactions with the extracellular matrix. *Cell Stem Cell* *5*, 17–26.
- Halder, G., Dupont, S., and Piccolo, S. (2012). Transduction of mechanical and cytoskeletal cues by YAP and TAZ. *Nat. Rev. Mol. Cell Biol.* *13*, 591–600.
- Heisenberg, C.-P., and Bellaïche, Y. (2013). Forces in tissue morphogenesis and patterning. *Cell* *153*, 948–962.

- Huang, D.W., Sherman, B.T., and Lempicki, R.A. (2009a). Bioinformatics enrichment tools: paths toward the comprehensive functional analysis of large gene lists. *Nucleic Acids Res.* *37*, 1–13.
- Huang, D.W., Sherman, B.T., and Lempicki, R.A. (2009b). Systematic and integrative analysis of large gene lists using DAVID bioinformatics resources. *Nature Protocols* *4*, 44–57.
- Kalkan, T., Olova, N., Roode, M., Mulas, C., Lee, H.J., Nett, I., Marks, H., Walker, R., Stunnenberg, H.G., Lilley, K.S., et al. (2017). Tracking the embryonic stem cell transition from ground state pluripotency. *Development* *144*, 1221–1234.
- Koser, D.E., Thompson, A.J., Foster, S.K., Dwivedy, A., Pillai, E.K., Sheridan, G.K., Svoboda, H., Viana, M., Costa, L. da F., Guck, J., et al. (2016). Mechanosensing is critical for axon growth in the developing brain. *Nature Neuroscience* *19*, 1592–1598.
- Kunath, T., Saba-El-Leil, M.K., Almousaillekh, M., Wray, J., Meloche, S., and Smith, A. (2007). FGF stimulation of the Erk1/2 signalling cascade triggers transition of pluripotent embryonic stem cells from self-renewal to lineage commitment. *Development* *134*, 2895–2902.
- Lieber, A.D., Yehudai-Resheff, S., Barnhart, E.L., Theriot, J.A., and Keren, K. (2013). Membrane Tension in Rapidly Moving Cells Is Determined by Cytoskeletal Forces. *Current Biology* *23*, 1409–1417.
- Liu, C., Li, Y., Semenov, M., Han, C., Baeg, G.-H., Tan, Y., Zhang, Z., Lin, X., and He, X. (2002). Control of β -Catenin Phosphorylation/Degradation by a Dual-Kinase Mechanism. *Cell* *108*, 837–847.
- Love, M.I., Huber, W., and Anders, S. (2014). Moderated estimation of fold change and dispersion for RNA-seq data with DESeq2. *Genome Biology* *15*, 550.
- Macia, E., Ehrlich, M., Massol, R., Boucrot, E., Brunner, C., and Kirchhausen, T. (2006). Dynasore, a Cell-Permeable Inhibitor of Dynamin. *Developmental Cell* *10*, 839–850.
- Matsui, T., Maeda, M., Doi, Y., Yonemura, S., Amano, M., Kaibuchi, K., Tsukita, S., and Tsukita, S. (1998). Rho-Kinase Phosphorylates COOH-terminal Threonines of Ezrin/Radixin/Moesin (ERM) Proteins and Regulates Their Head-to-Tail Association. *J Cell Biol* *140*, 647–657.
- McBeath, R., Pirone, D.M., Nelson, C.M., Bhadriraju, K., and Chen, C.S. (2004). Cell shape, cytoskeletal tension, and RhoA regulate stem cell lineage commitment. *Dev. Cell* *6*, 483–495.
- Mendoza, P., Díaz, J., Silva, P., and Torres, V.A. (2014). Rab5 activation as a tumor cell migration switch. *Small GTPases* *5*, e28195.
- Molotkov, A., Mazot, P., Brewer, J.R., Cinalli, R.M., and Soriano, P. (2017). Distinct Requirements for FGFR1 and FGFR2 in Primitive Endoderm Development and Exit from Pluripotency. *Developmental Cell* *41*, 511–526.e4.

- Mulas, C., Kalkan, T., Meyenn, F. von, Leitch, H.G., Nichols, J., and Smith, A. (2019). Defined conditions for propagation and manipulation of mouse embryonic stem cells. *Development* *146*, dev173146.
- Murray, P., Prewitz, M., Hopp, I., Wells, N., Zhang, H., Cooper, A., Parry, K.L., Short, R., Antoine, D.J., and Edgar, D. (2013). The self-renewal of mouse embryonic stem cells is regulated by cell–substratum adhesion and cell spreading. *Int J Biochem Cell Biol* *45*, 2698–2705.
- Nambiar, R., McConnell, R.E., and Tyska, M.J. (2009). Control of cell membrane tension by myosin-I. *PNAS* *106*, 11972–11977.
- Nett, I.R., Mulas, C., Gatto, L., Lilley, K.S., and Smith, A. (2018). Negative feedback via RSK modulates Erk- dependent progression from naïve pluripotency. *EMBO Reports* e45642.
- Nichols, J., Silva, J., Roode, M., and Smith, A. (2009). Suppression of Erk signalling promotes ground state pluripotency in the mouse embryo. *Development* *136*, 3215–3222.
- Palamidessi, A., Malinverno, C., Frittoli, E., Corallino, S., Barbieri, E., Sigismund, S., Beznoussenko, G.V., Martini, E., Garre, M., Ferrara, I., et al. (2019). Unjamming overcomes kinetic and proliferation arrest in terminally differentiated cells and promotes collective motility of carcinoma. *Nat. Mater.* 1–12.
- Paluch, E., and Heisenberg, C.-P. (2009). Biology and Physics of Cell Shape Changes in Development. *Current Biology* *19*, R790–R799.
- Pepe-Mooney, B.J., Dill, M.T., Alemany, A., Ordovas-Montanes, J., Matsushita, Y., Rao, A., Sen, A., Miyazaki, M., Anakk, S., Dawson, P.A., et al. (2019). Single-Cell Analysis of the Liver Epithelium Reveals Dynamic Heterogeneity and an Essential Role for YAP in Homeostasis and Regeneration. *Cell Stem Cell* *25*, 23-38.e8.
- Pertz, O., Hodgson, L., Klemke, R.L., and Hahn, K.M. (2006). Spatiotemporal dynamics of RhoA activity in migrating cells. *Nature* *440*, 1069–1072.
- Platta, H.W., and Stenmark, H. (2011). Endocytosis and signaling. *Current Opinion in Cell Biology* *23*, 393–403.
- Pontes, B., Monzo, P., and Gauthier, N.C. (2017a). Membrane tension: A challenging but universal physical parameter in cell biology. *Semin. Cell Dev. Biol.* *71*, 30–41.
- Pontes, B., Monzo, P., Gole, L., Le Roux, A.-L., Kosmalska, A.J., Tam, Z.Y., Luo, W., Kan, S., Viasnoff, V., Roca-Cusachs, P., et al. (2017b). Membrane tension controls adhesion positioning at the leading edge of cells. *J. Cell Biol.* *216*, 2959–2977.
- Pouille, P.-A., Ahmadi, P., Brunet, A.-C., and Farge, E. (2009). Mechanical Signals Trigger Myosin II Redistribution and Mesoderm Invagination in *Drosophila* Embryos. *Sci. Signal.* *2*, ra16–ra16.

- Przybyla, L., Lakins, J.N., and Weaver, V.M. (2016). Tissue Mechanics Orchestrate Wnt-Dependent Human Embryonic Stem Cell Differentiation. *Cell Stem Cell* *19*, 462–475.
- Rappaport, J., Manthe, R.L., Solomon, M., Garnacho, C., and Muro, S. (2016). A Comparative Study on the Alterations of Endocytic Pathways in Multiple Lysosomal Storage Disorders. *Mol Pharm* *13*, 357–368.
- Rauch, C., Brunet, A.-C., Deleule, J., and Farge, E. (2002). C2C12 myoblast/osteoblast transdifferentiation steps enhanced by epigenetic inhibition of BMP2 endocytosis. *Am. J. Physiol., Cell Physiol.* *283*, C235-243.
- Raucher, D., and Sheetz, M.P. (2000). Cell Spreading and Lamellipodial Extension Rate Is Regulated by Membrane Tension. *J Cell Biol* *148*, 127–136.
- Razzell, W., Wood, W., and Martin, P. (2014). Recapitulation of morphogenetic cell shape changes enables wound re-epithelialisation. *Development* *141*, 1814–1820.
- Riedl, J., Flynn, K.C., Raducanu, A., Gärtner, F., Beck, G., Bösl, M., Bradke, F., Massberg, S., Aszodi, A., Sixt, M., et al. (2010). Lifeact mice for studying F-actin dynamics. *Nat. Methods* *7*, 168–169.
- Rouven Brückner, B., Pietuch, A., Nehls, S., Rother, J., and Janshoff, A. (2015). Ezrin is a Major Regulator of Membrane Tension in Epithelial Cells. *Scientific Reports* *5*, 14700.
- Schindelin, J., Arganda-Carreras, I., Frise, E., Kaynig, V., Longair, M., Pietzsch, T., Preibisch, S., Rueden, C., Saalfeld, S., Schmid, B., et al. (2012). Fiji: an open-source platform for biological-image analysis. *Nature Methods* *9*, 676–682.
- Segel, M., Neumann, B., Hill, M.F.E., Weber, I.P., Viscomi, C., Zhao, C., Young, A., Agley, C.C., Thompson, A.J., Gonzalez, G.A., et al. (2019). Niche stiffness underlies the ageing of central nervous system progenitor cells. *Nature*.
- Solis, A.G., Bielecki, P., Steach, H.R., Sharma, L., Harman, C.C.D., Yun, S., de Zoete, M.R., Warnock, J.N., To, S.D.F., York, A.G., et al. (2019). Mechanosensation of cyclical force by PIEZO1 is essential for innate immunity. *Nature* *573*, 69–74.
- Solter, D., and Knowles, B.B. (1975). Immunosurgery of mouse blastocyst. *PNAS* *72*, 5099–5102.
- Sorkin, A., and von Zastrow, M. (2009). Endocytosis and signalling: intertwining molecular networks. *Nature Reviews Molecular Cell Biology* *10*, 609–622.
- Tee, S.-Y., Fu, J., Chen, C.S., and Janmey, P.A. (2011). Cell Shape and Substrate Rigidity Both Regulate Cell Stiffness. *Biophysical Journal* *100*, L25.
- Thottacherry, J.J., Kosmalska, A.J., Kumar, A., Vishen, A.S., Elosegui-Artola, A., Pradhan, S., Sharma, S., Singh, P.P., Guadamillas, M.C., Chaudhary, N., et al. (2018). Mechanochemical

feedback control of dynamin independent endocytosis modulates membrane tension in adherent cells. *Nat Commun* 9, 4217.

Totaro, A., Castellan, M., Battilana, G., Zanconato, F., Azzolin, L., Giulitti, S., Cordenonsi, M., and Piccolo, S. (2017). YAP/TAZ link cell mechanics to Notch signalling to control epidermal stem cell fate. *Nature Communications* 8, 1–13.

Turner, D.A., Girgin, M., Alonso-Crisostomo, L., Trivedi, V., Baillie-Johnson, P., Glodowski, C.R., Hayward, P.C., Collignon, J., Gustavsen, C., Serup, P., et al. (2017). Anteroposterior polarity and elongation in the absence of extra-embryonic tissues and of spatially localised signalling in gastruloids: mammalian embryonic organoids. *Development* 144, 3894–3906.

Verstreken, C.M., Labouesse, C., Agle, C.C., and Chalut, K.J. (2019). Embryonic stem cells become mechanoresponsive upon exit from ground state of pluripotency. *Open Biol.* 9, 180203.

Wray, J., Kalkan, T., Gomez-Lopez, S., Eckardt, D., Cook, A., Kemler, R., and Smith, A. (2011). Inhibition of glycogen synthase kinase-3 alleviates Tcf3 repression of the pluripotency network and increases embryonic stem cell resistance to differentiation. *Nature Cell Biology* 13, 838–845.

Wu, T.D., and Nacu, S. (2010). Fast and SNP-tolerant detection of complex variants and splicing in short reads. *Bioinformatics* 26, 873–881.

Yanagida, A., Revell, C., Stirparo, G.G., Corujo-Simon, E., Aspalter, I.M., Peters, R., Belly, H.D., Cassani, D.A.D., Achouri, S., Blumenfeld, R., et al. (2020). Cell surface fluctuations regulate early embryonic lineage sorting. *BioRxiv* 2020.08.16.250084.

Ying, Q.-L., Wray, J., Nichols, J., Batlle-Morera, L., Doble, B., Woodgett, J., Cohen, P., and Smith, A. (2008). The ground state of embryonic stem cell self-renewal. *Nature* 453, 519–523.

Yui, S., Azzolin, L., Maimets, M., Pedersen, M.T., Fordham, R.P., Hansen, S.L., Larsen, H.L., Guiu, J., Alves, M.R.P., Rundsten, C.F., et al. (2018). YAP/TAZ-Dependent Reprogramming of Colonic Epithelium Links ECM Remodeling to Tissue Regeneration. *Cell Stem Cell* 22, 35–49.e7.

Figure 1

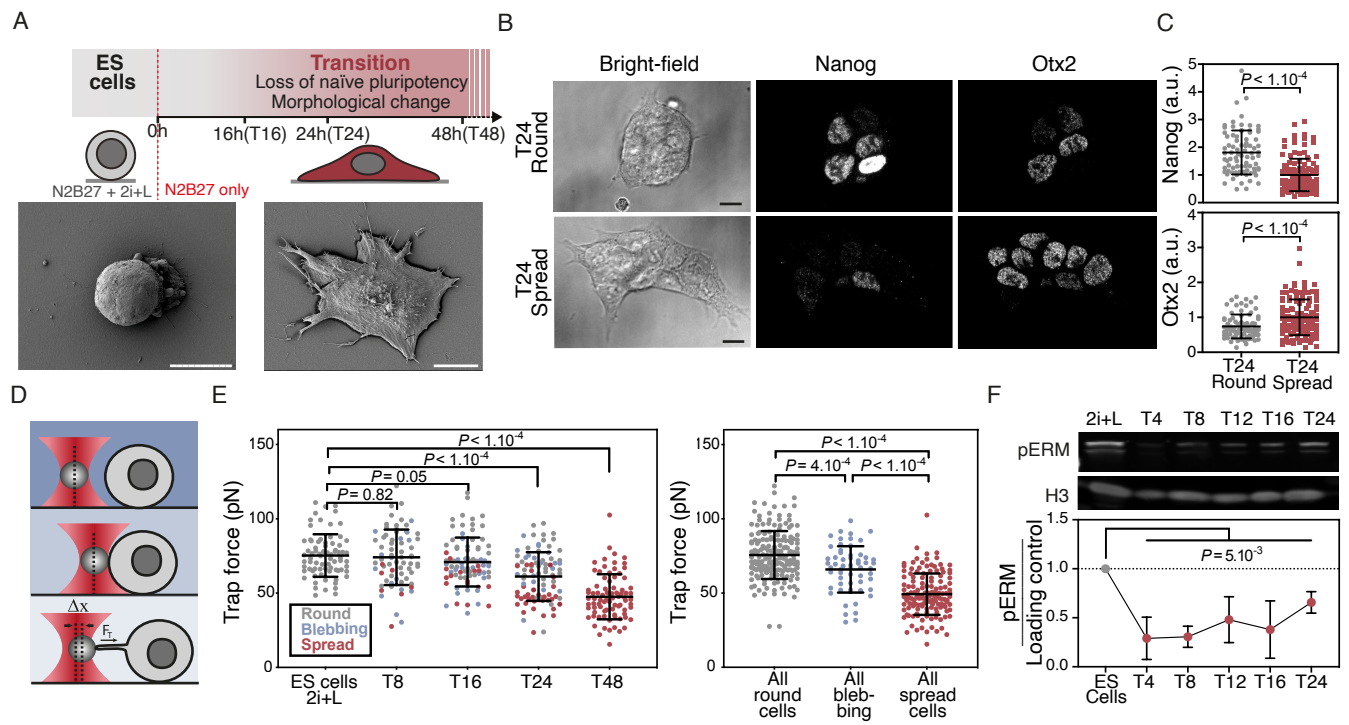


Figure 2

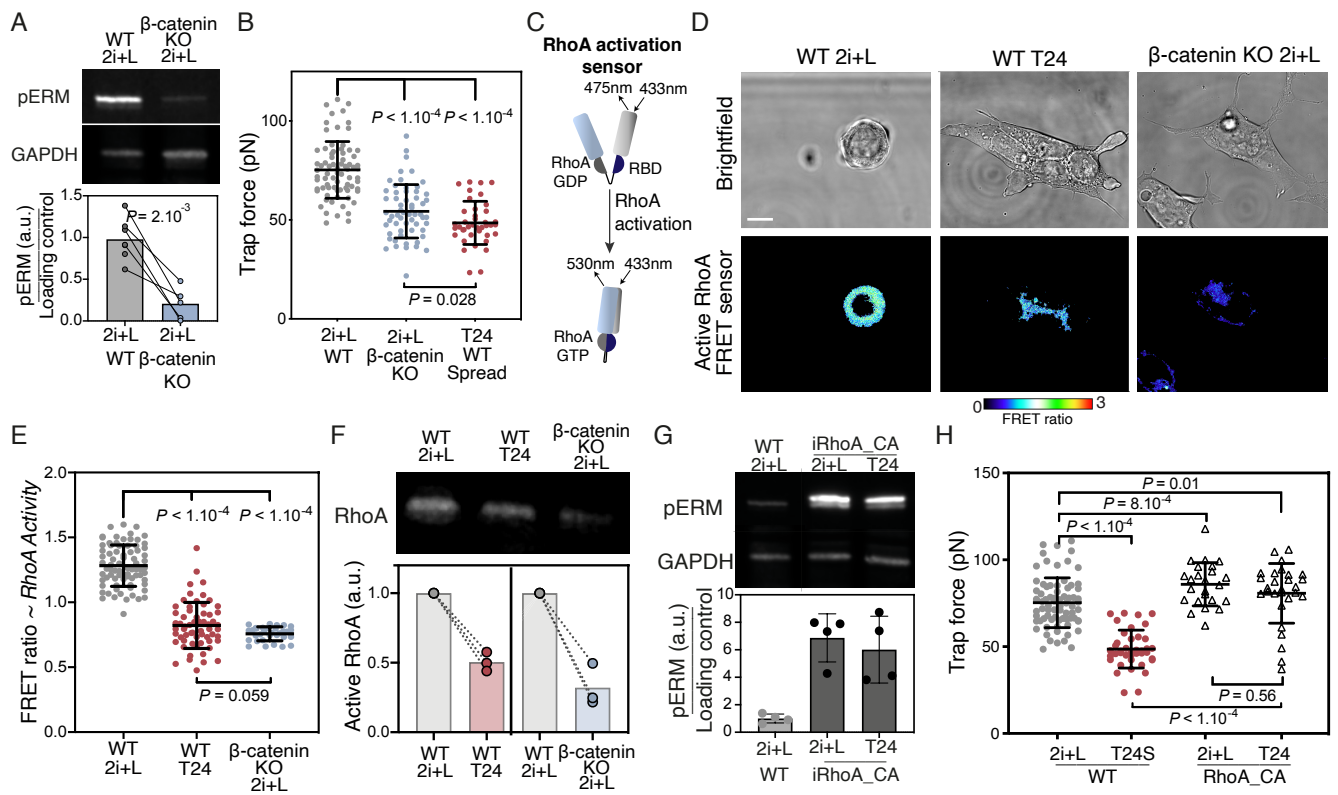


Figure 3

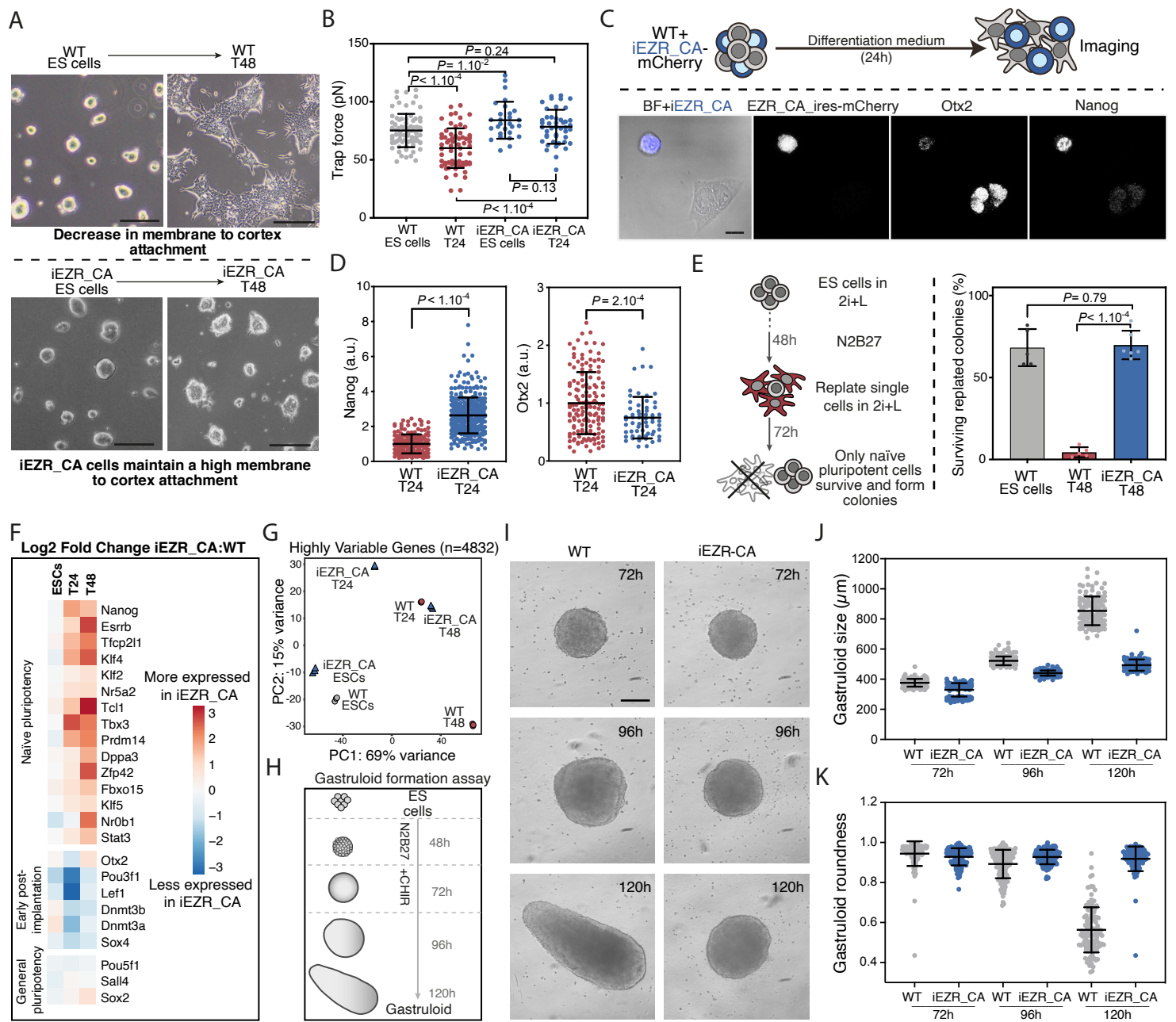


Figure 4

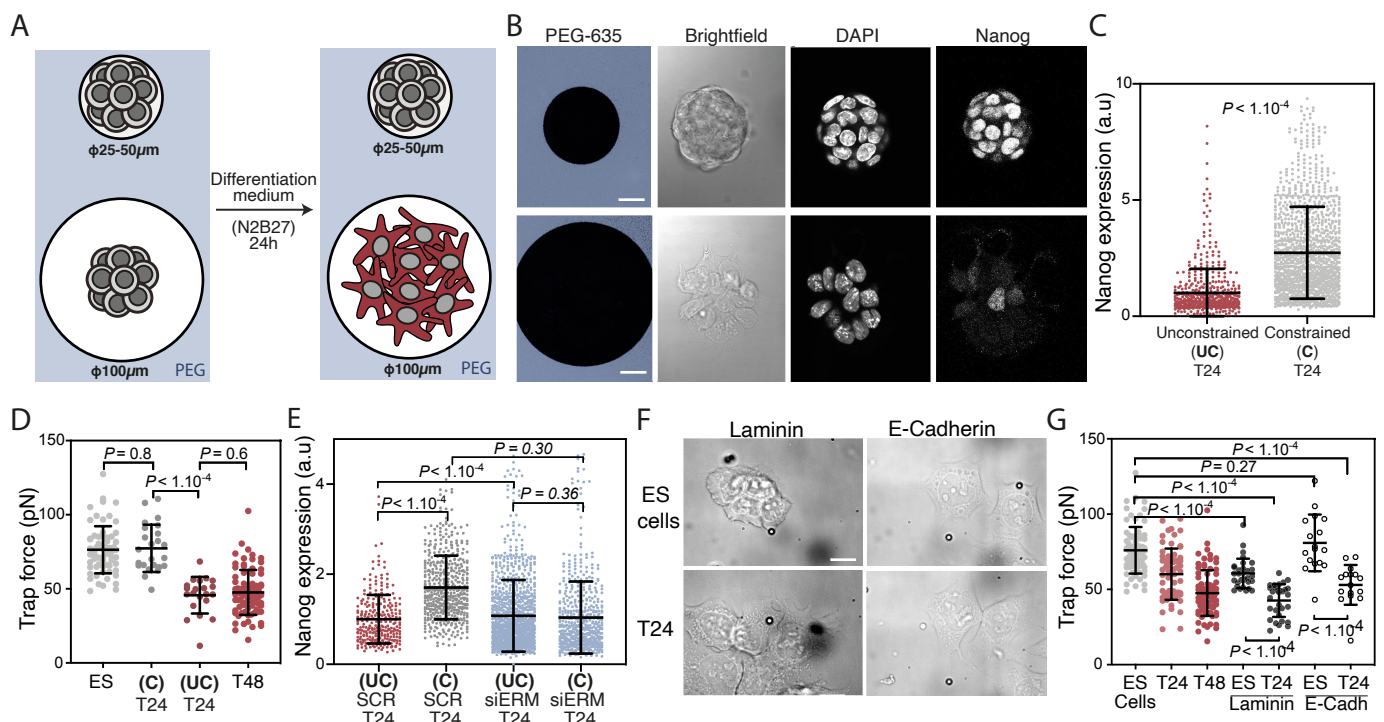


Figure 5

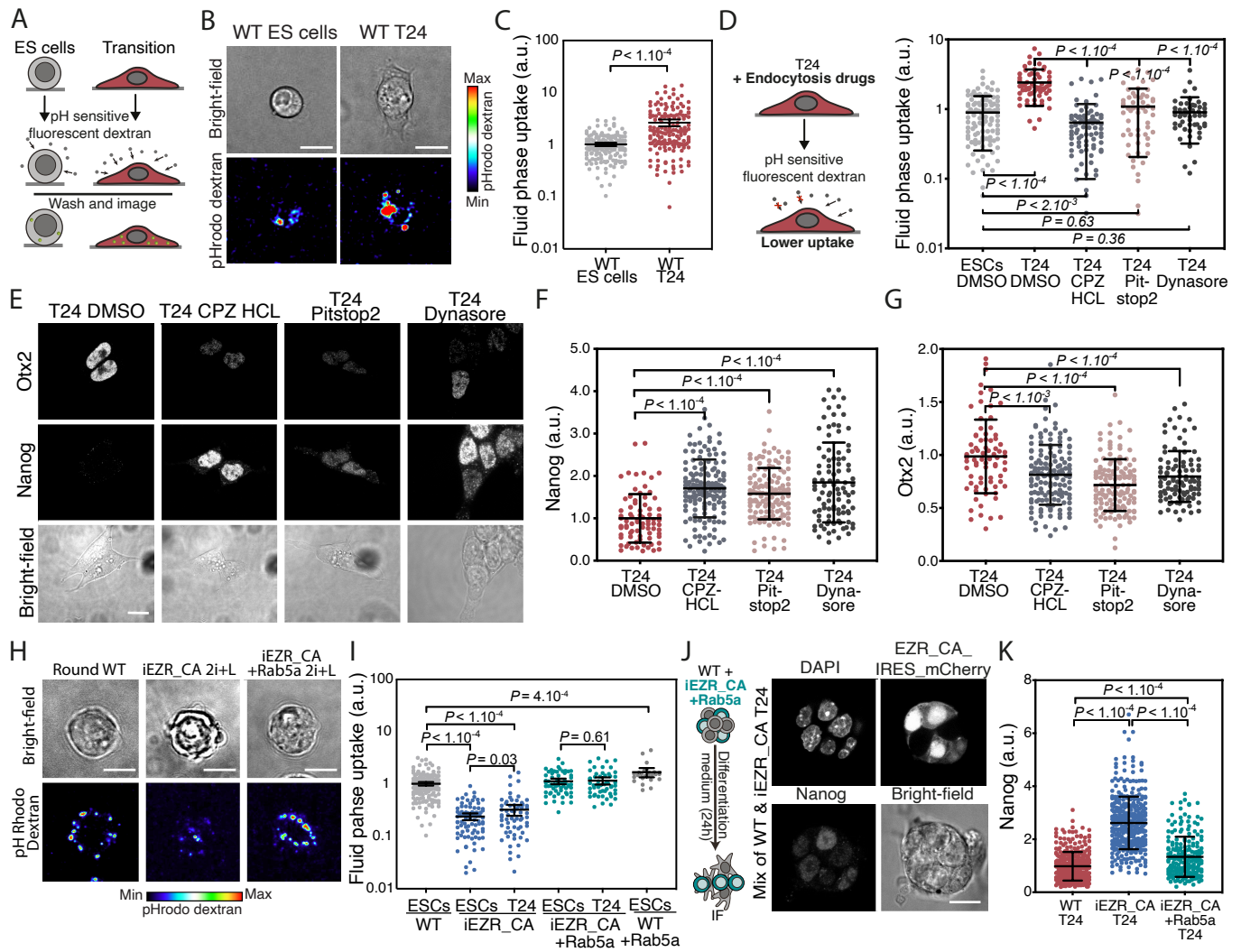
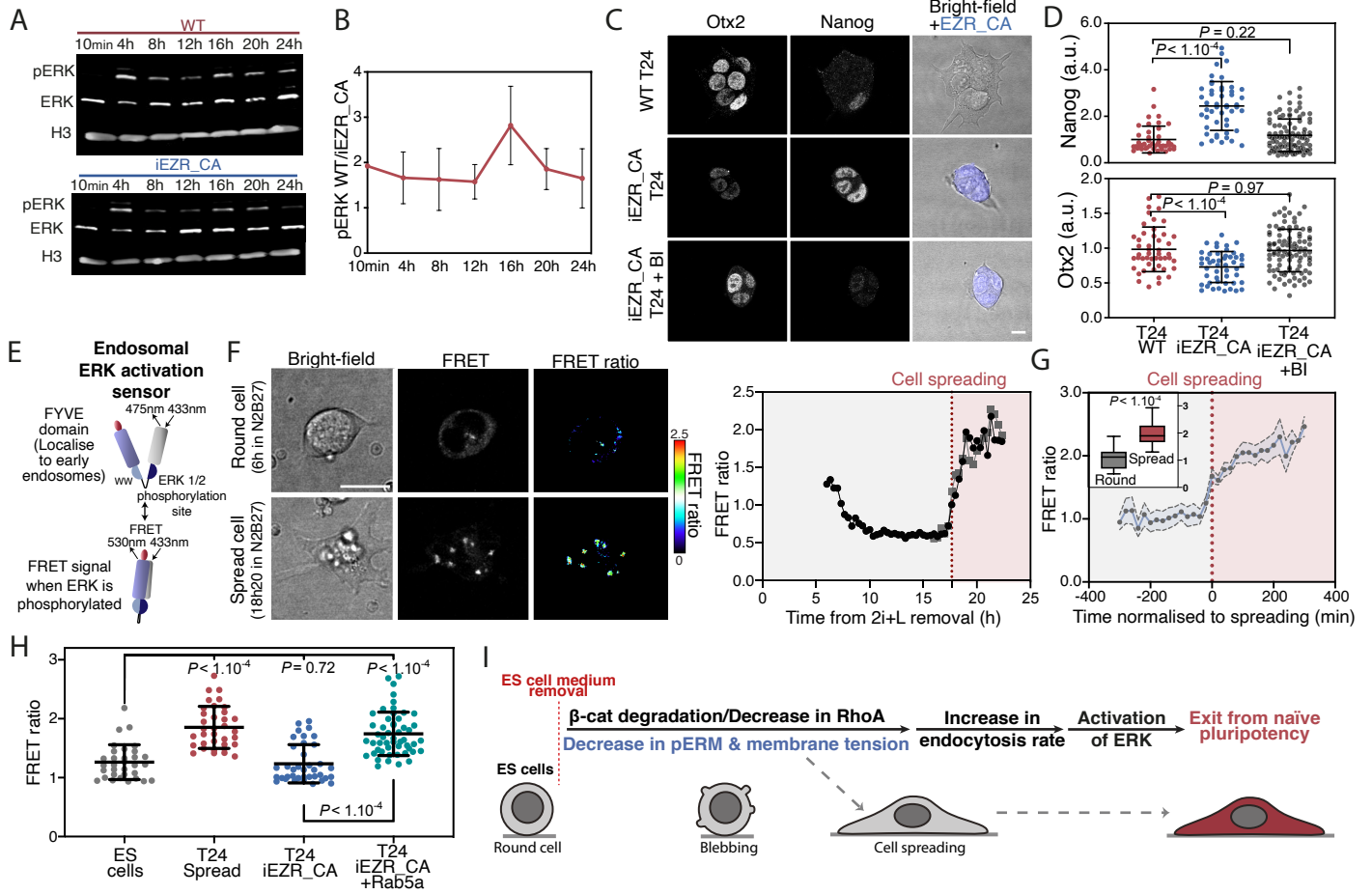


Figure 6



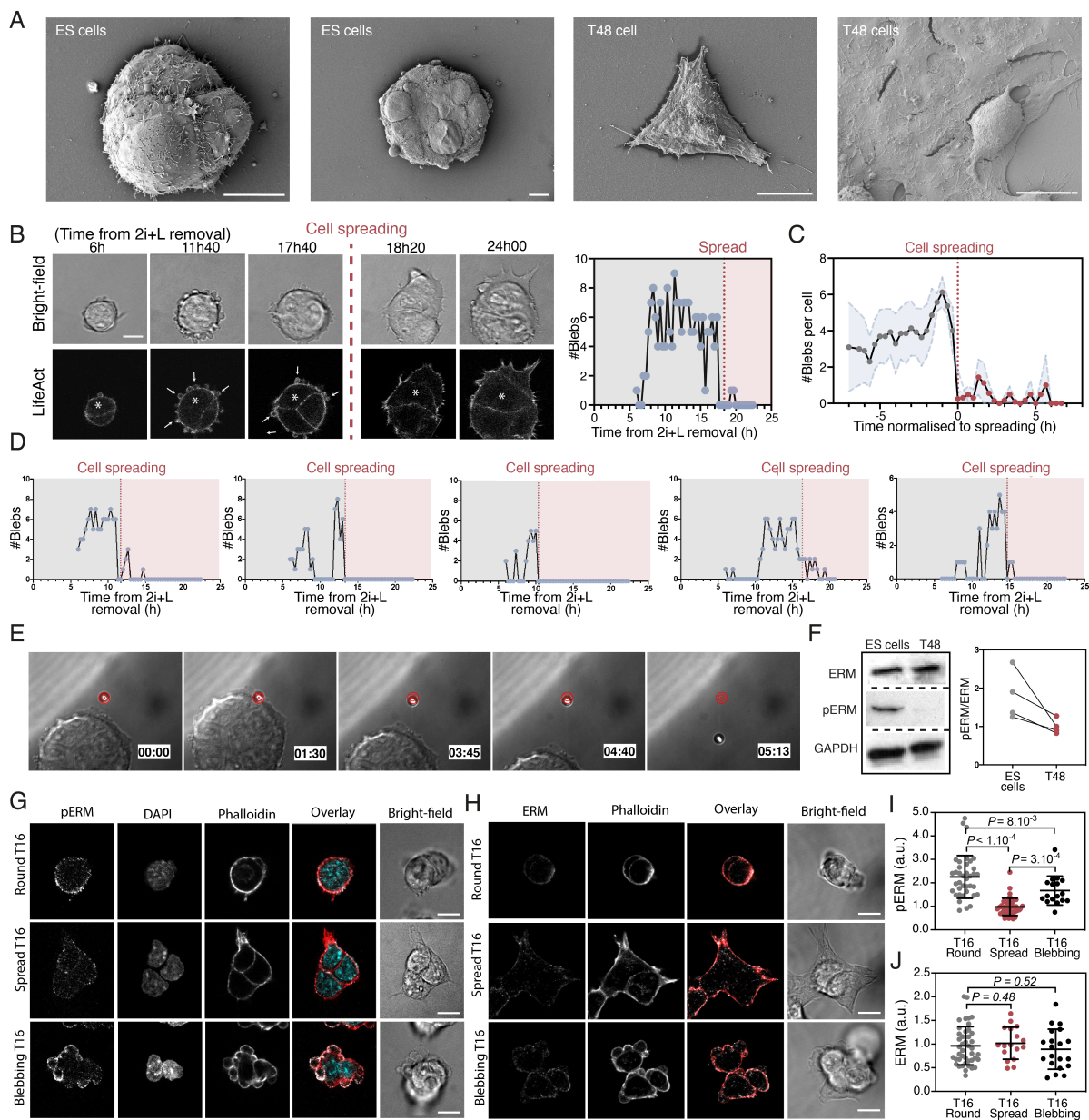


Figure S1: Membrane to cortex attachment and membrane tension are decreased during early differentiation (related to Figure 1). **A**, Representative SEM images of ES and T48 cells. Scale bars, 10 μm . **B**, Left: time-lapse of representative ES cells expressing LifeAct-GFP and exiting naïve pluripotency. White arrows: cellular blebs. Red dotted line indicates approximate time of cell spreading. Right: quantification of the number of blebs in the cell marked with a white star. **C**, Quantification of cell blebbing during exit from naïve pluripotency. Time is normalised to the time of spreading (mean \pm SD, $n = 20$, $N=2$). **D**, Quantification of blebbing in six different ES cells expressing LifeAct-GFP during exiting naïve pluripotency. Red dotted line indicates approximate time of cell spreading. Bleb numbers per cell significantly decrease once the cell is spread (pink shaded area). **E**, Time lapse of a membrane tension measurement in a colony of ES cell. Time is in minutes:seconds. A red target is placed at the centre of the trap to help visualize bead displacement. **F**, Representative western blot for ERM, pERM and GAPDH in ES

cells and T24 cells and corresponding quantification (N=4, lines connect data points from individual experiments) **G**, Images of a single z-plane in fixed T16 cells. Three different cell morphologies are observed at T16: round, spread and blebbing. Cells were immunostained for pERM, and stained with DAPI and phalloidin. **H**, Similar as D with ERM instead of pERM. **I, J**, Estimated pERM and ERM and density in round, spread and blebbing T16 cells. Protein density was estimated from the mean intensity of sum z projections, corrected for background, and normalised to the mean of T16 round cells. (Means \pm SD, N=3). For all panels, unless otherwise indicated, p-values established by Welch's unpaired student t-test.

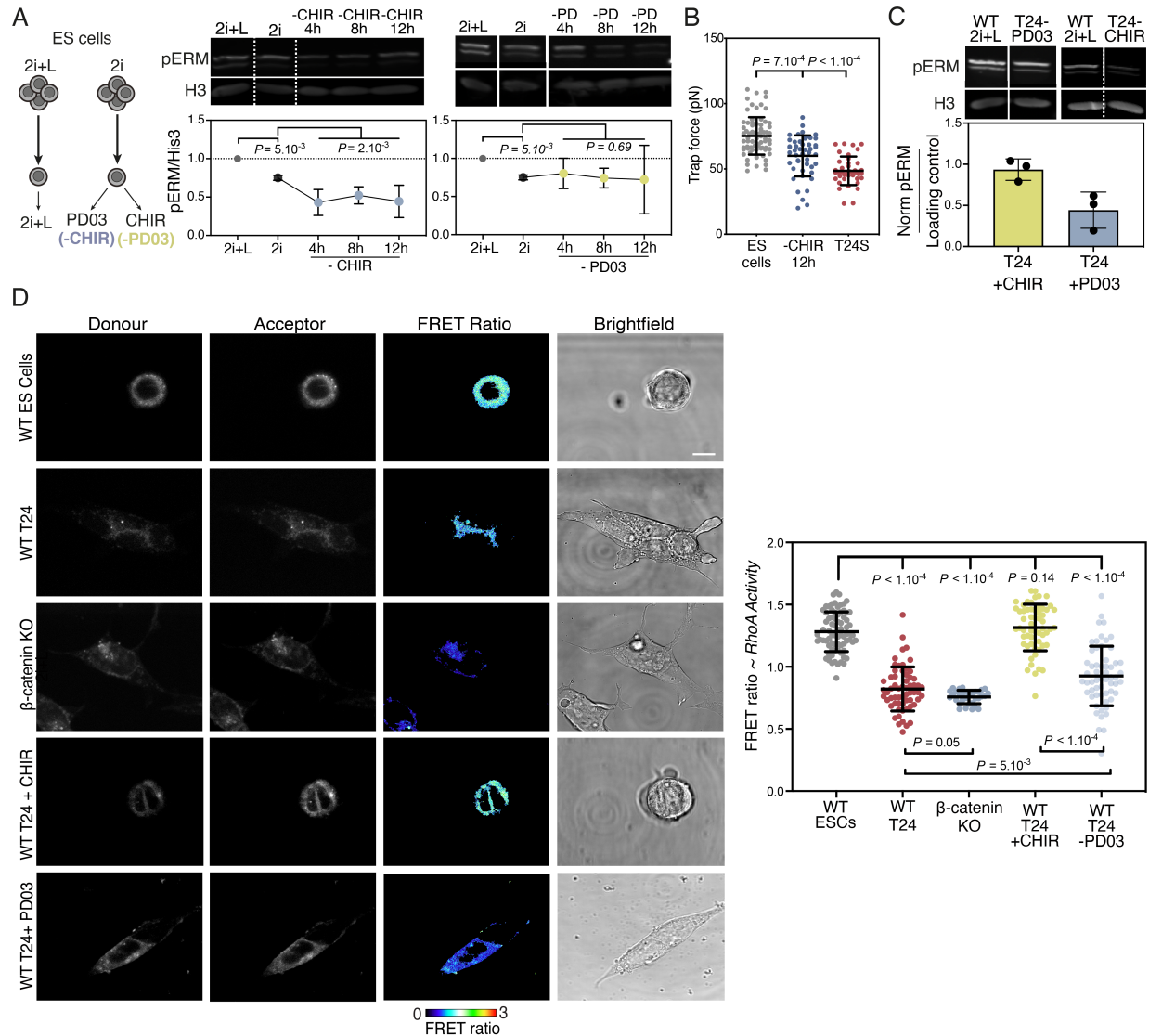


Figure S2: pERM activity and membrane tension during early differentiation are regulated by β -catenin and RhoA (related to Figure 2). **A**, Fluorescent Western Blot and associated quantification for pERM and Histone 3 (his 3) of cells cultured in 2i+L or from 2i and replated with PD03 or CHIR only for various timepoints (N=5). *P* values are calculated using a two-way analysis of variance (ANOVA), using experiment repeats and medium condition as variables, and indicated in the figure. **B**, Trap force measurements of WT ES, T24S (from Figure 1E) and cells cultured in medium lacking Chir (from 2i) (N=3). **C**, Top, representative fluorescent western blots for phospho-ERM and His3 of ES cells and T24 cells cultured in differentiation medium from 2i+L with either CHIR (annotated -PD03) or PD03 (annotated -CHIR). Bottom, associated quantification (N=3). **D**, Left, representative images of WT ES, T24, β -catenin KO cells and cells from 2i+L cultured for 24h in differentiation medium (N2B27) containing either PD03 (annotated -CHIR) or CHIR (annotated -PD03). Right, associated quantification (N=3). Graphical data represents mean \pm SD. *P* values are calculated by Welch's unpaired student t-test (unless otherwise indicated). Scale bars = 10 μ m.

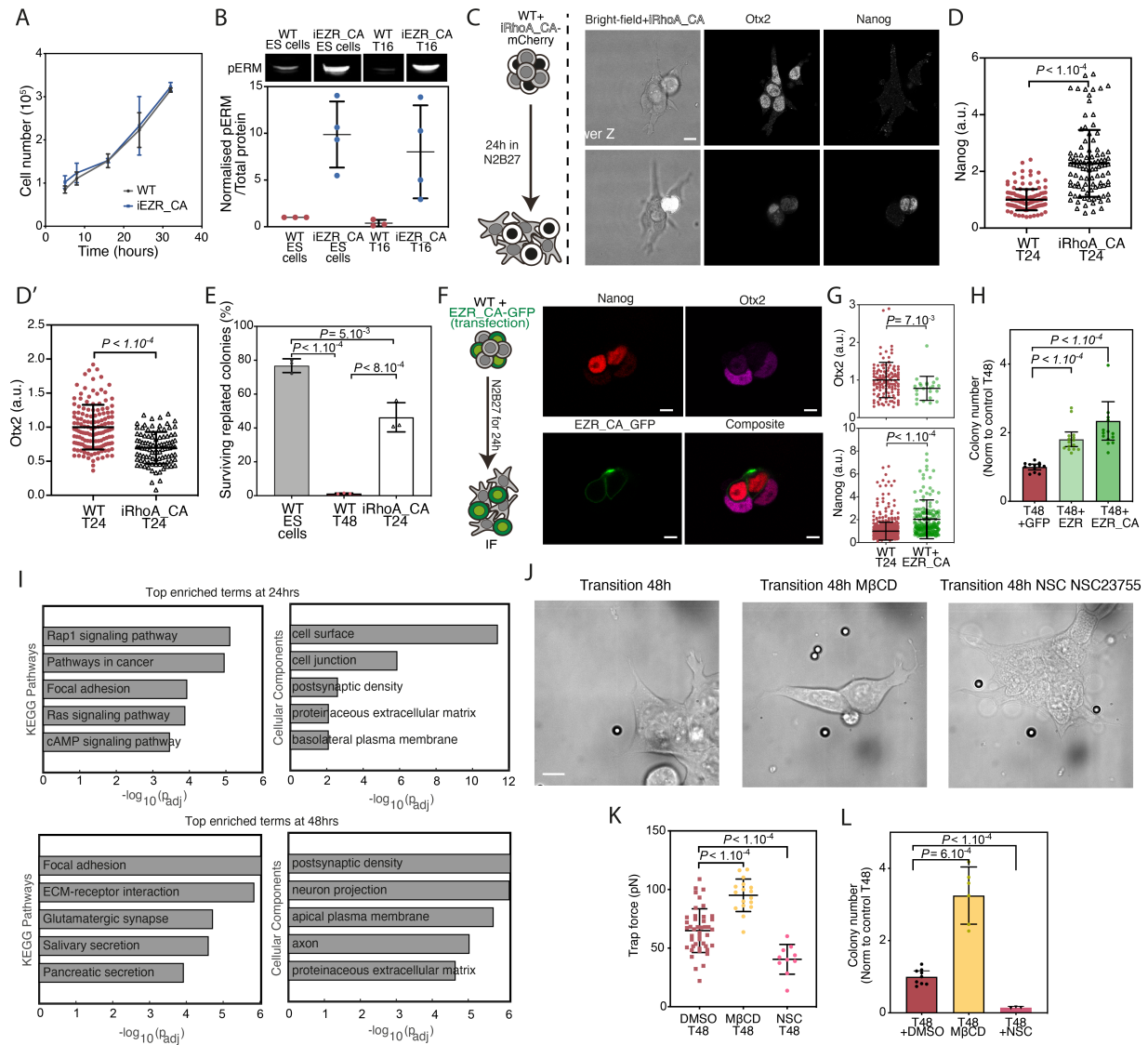


Figure S3: Increasing membrane tension inhibits early differentiation (related to Figure 3). **A**, Proliferation curves of WT and iEZR_CA ES cells (N=3). **B**, Quantification of phospho-ERM normalised to total protein levels in WT and iEZR_CA ES and T16 cells. Data are normalised to the mean of WT ES cells (N=4). **C**, Representative images of two z plane of a mix of WT and iRhoA_CA T24 cells immunostained for Otx2 and Nanog. **D**, Quantification of Nanog and Otx2 expression in WT and iRhoA_CA T24 cells, normalised to WT mean levels (N=3). **E**, Left, schematic of clonogenicity assay used as a measure of naïve pluripotency. Right: quantification of the percentage of surviving replated cells in a clonogenicity assay using WT and iRhoA_CA cells. Cells replated directly from 2i+L are used as a positive control (N=3). **F**, Representative single z-planes of a mix of control and EZR_CA transfected (positive for the EZR_CA_GFP) T24 cells immunostained for Otx2 and Nanog. **G**, Quantification of Nanog and Otx2 expression in T24 cells transfected or not with EZR_CA_GFP, normalised to T24 control mean

(N=2). **H**, Quantification of surviving replated cells in a clonogenicity assay using T48 cells transfected with either GFP (control), EZR, EZR_CA. (N=4) **I**, Top 5 KEGG pathways terms and Cellular Components terms that are enriched in the differentially regulated genes (n = 1165 genes at T24 and n = 1922 genes at T48). A threshold of > 5 was used for mean log₂ expression, of ≥ 2.0 for fold enrichment, and of > 1% for proportion of regulated in each annotation. Adjusted p-value threshold was set at 0.1. The enriched annotations were sorted on increasing p-value and the top 5 were selected. **J**, Representative images of T48 cells treated with DMSO, NSC23766 or M β CD. M β CD was used at 1 mM for 1 h every 24 h. NSC23766 was used at 25 μ M for 1 h every 24 h (N=3). **K**, Trap force measurements of T48 cells treated with DMSO, NSC23766 or M β CD at similar concentrations as in J. (N=2). **L**, Clonogenicity assay used to measure efficiency of exit from naïve pluripotency using T48 cells and different treatments to affect membrane tension. T48 cells replated from N2B27+DMSO were used as control for drug treatment. (N=3). Graphical data represents mean \pm SD unless specified otherwise. Each condition is normalised to their respective control. *P* values are calculated by Welch's unpaired student t-test. Scale bars = 10 μ m.

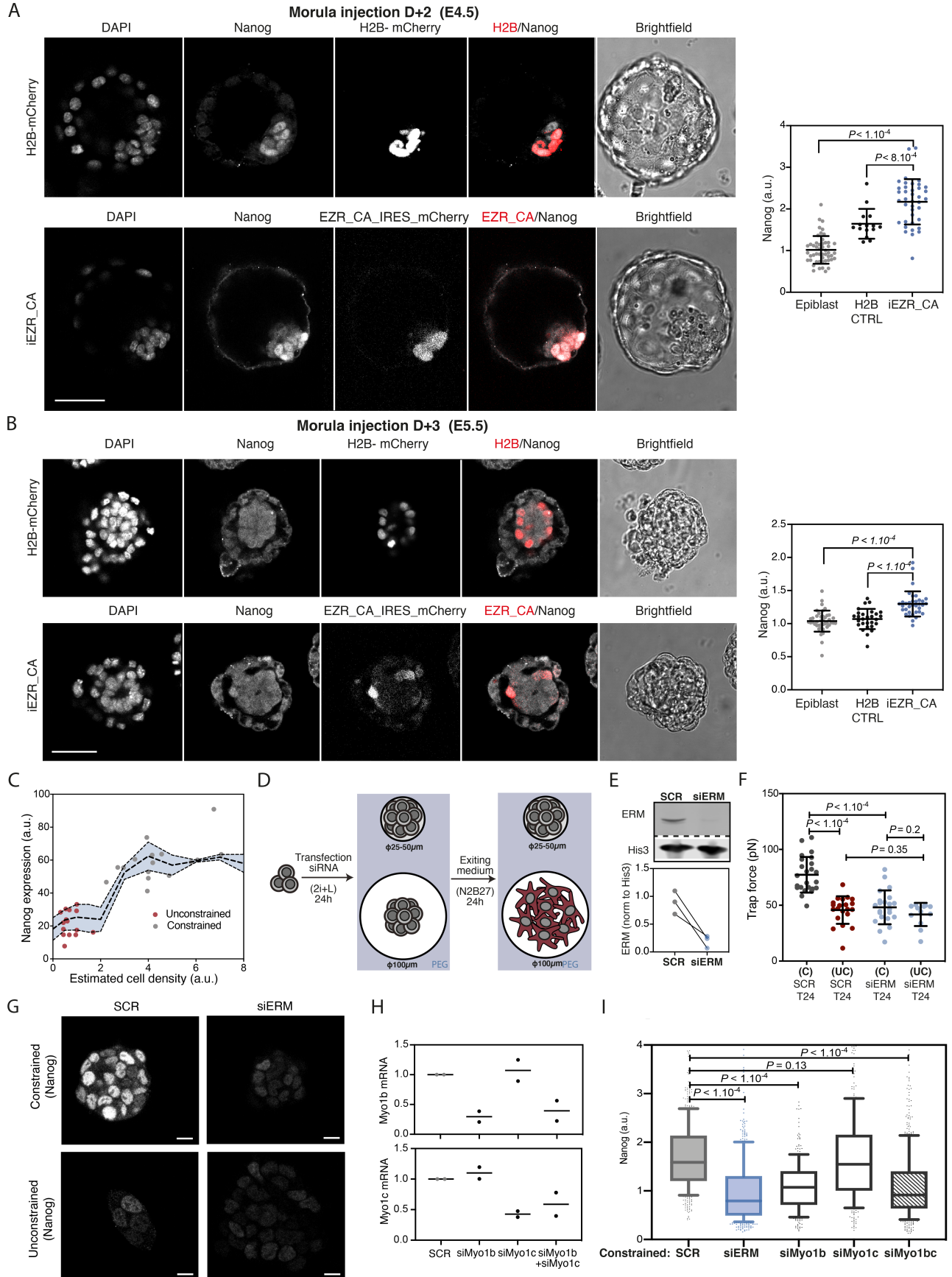


Figure S4: Maintaining a high membrane tension impairs exit from naïve pluripotency independently of cell shape (related to Figure 4).

A, B, Representative images and associated quantification of morula injection experiment in which either control cells (H2B-mCherry) or iEZR_CA were injected at the 8 cells stage into the mouse embryo, which was then maintained in culture for 48 or 72h (see methods for details) (N=2). **C,** Same Nanog expression as in Figure 4C plotted in function of estimated cell density. Cell density was estimated by counting the number of cells and dividing by the pattern area. Data are colored based on size of pattern (red for 100 μm diameter and grey for 25-50 μm diameter). **D,** Schematic of the micropatterning assay combined with transfection of plasmids or siRNA. **E,** Fluorescent Western blot (inverted contrast) for ERM and Histone 3 in cells transfected with siSCR and siERM showing the efficiency of the knockdown. **F,** Trap force measurement of cells cultured on micropatterns and transfected or not with siRNA against ERM proteins. (N=2). **G,** Representative images of single z-planes in fixed T24 cells treated with either SCR or ERM siRNA and cultured on micropatterns. **H,** Quantification of Myo1b and Myo1c RNA by qPCR assay in ES cells treated with either SCR, siMyo1b, siMyo1c and siMyo1b+siMyo1c. Data were normalised to Actb expression. **I,** Boxes and whiskers with 10-90 percentile plot of Nanog expression of T24 cells either transfected with siMyo1b, siMyo1c or siMyo1b+siMyo1c. Only data for cells constrained on small micropatterns are shown. *P* values are calculated by Mann-Whitney U here. Graphical data represents mean \pm SD unless specified otherwise. *P* values are calculated by Welch's unpaired student t-test unless specified otherwise. Scale bars = 10 μm .

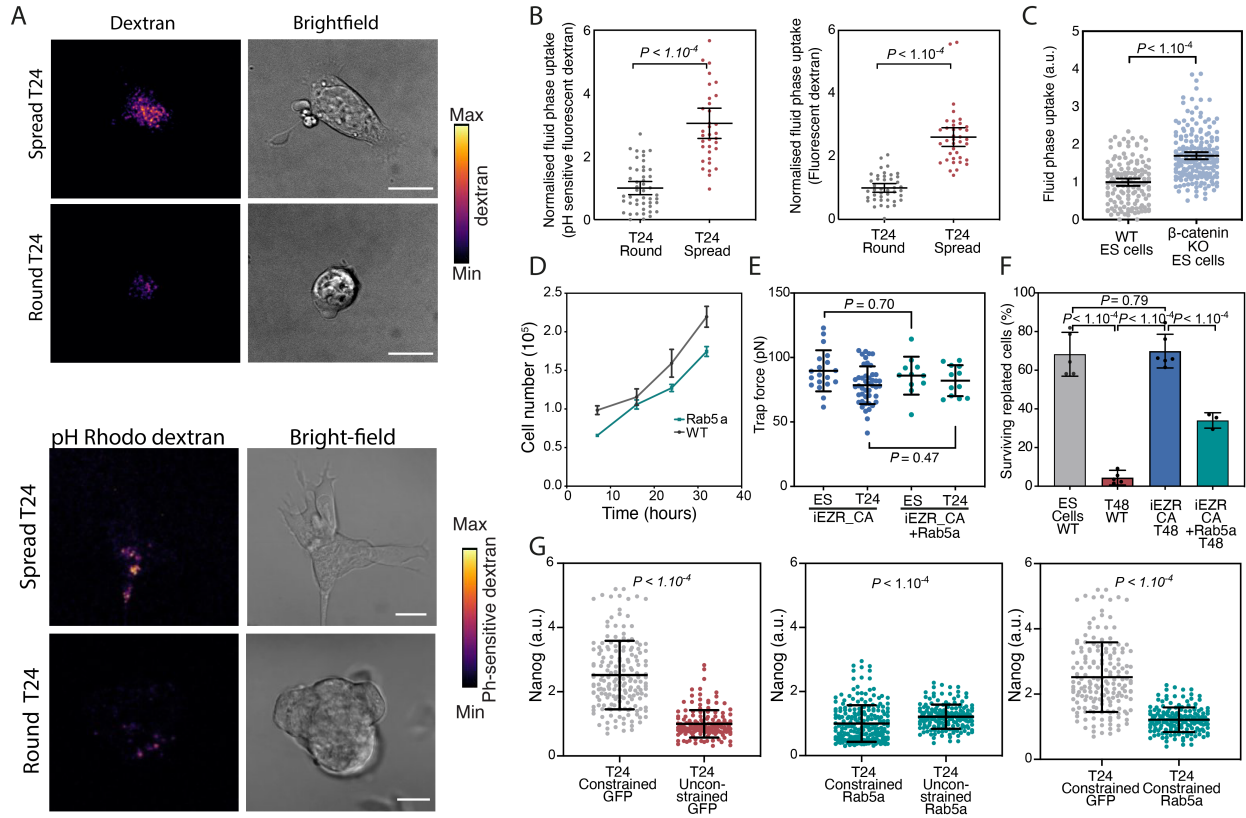


Figure S5: Endocytosis levels regulate exit from naïve pluripotency (related to Figure 5). **A**, Representative images of sum z-projections in round and spread T24 cells during a liquid phase uptake assay using fluorescent dextran or pH-sensitive fluorescent dextran. **B**, Left, quantification of liquid phase uptake using fluorescent dextran or pH-sensitive fluorescent dextran in T24 cells. Data are separated based on cell shape (round or spread). (Mean \pm 95% Confidence Interval, N=2). **C**, Quantification of fluid phase uptake assay of WT & β -catenin KO ES cells. Data are normalised to WT ES cells average (N=3). **D**, Proliferation curves of WT and WT+Rab5a cells (N=2). **E**, Trap force measurements of iEZR_CA cells transfected with Rab5a, iEZR_CA trap force data are from Figure 3B. (N=2). **F**, Quantification of the percentage of surviving replated cells in a clonogenicity assay using ES and T48 cells, WT or iEZR_CA, transfected or not with Rab5a. Data for iEZR_CA T48 cells are from Figure 3E. (N=3). **G**, Quantification of Nanog expression of fixed T24 cells transfected with GFP as control or Rab5a, cultured on micropatterns. This shows that Rab5a transfection can also rescue exit defects in constrained cells cultured on micropatterns. Data are normalised to cells cultured on 100 μ m diameter patterns (Unconstrained) (P values in this panel are calculated by Mann-Whitney U test; N=3). Graphical data represents mean \pm SD unless specified otherwise. P values are calculated by Welch's unpaired student t-test (unless specified otherwise) and are indicated in the figure. Scale bars = 10 μ m.

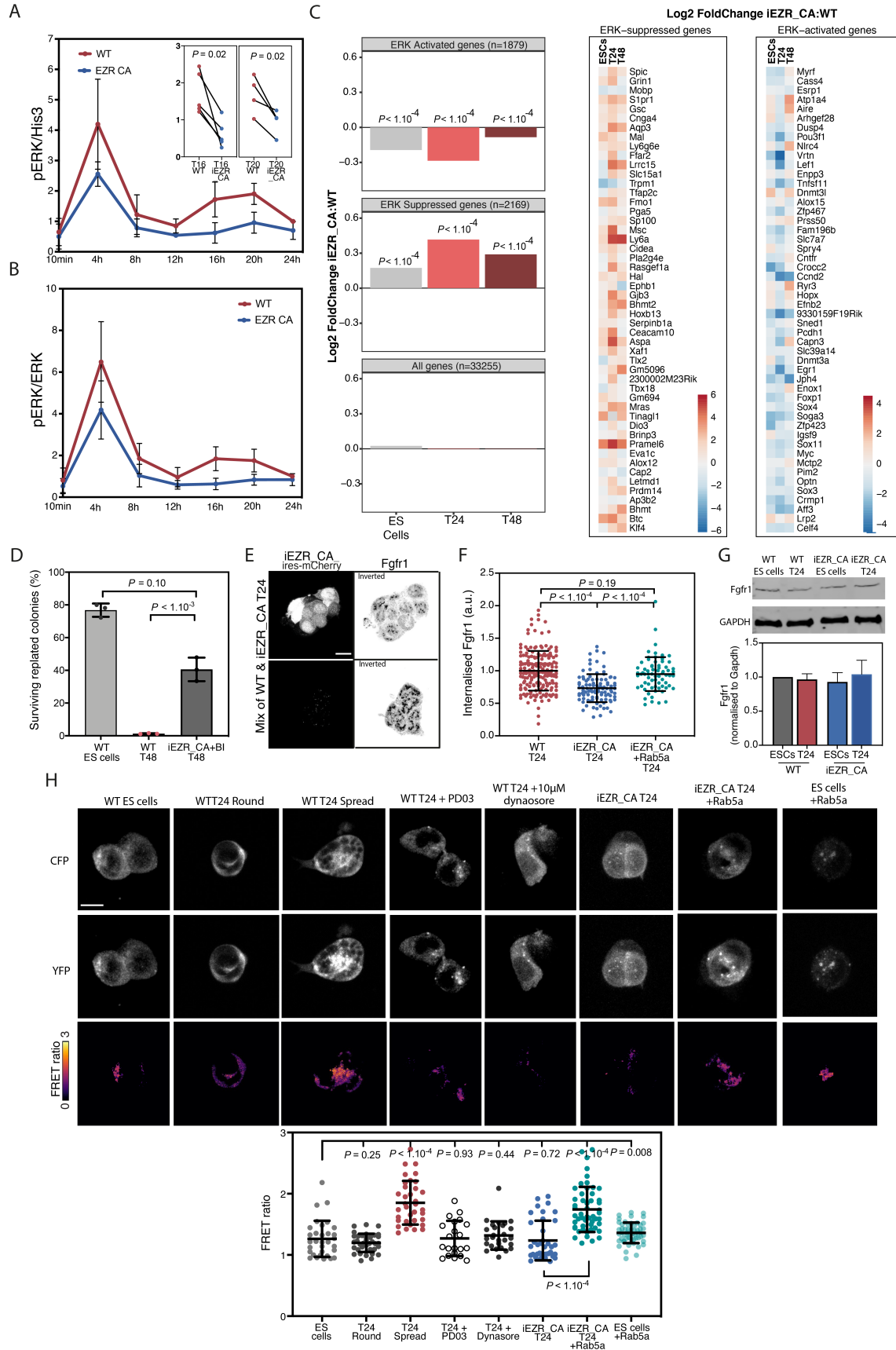


Figure S6: ERK signalling and FGFR1 expression in exit from naïve pluripotency (related to Figure 6).

A, Quantification of phospho-ERK normalised to Histone 3 levels across several fluorescent Western blots (including Figure 6A) done on WT and iEZR_CA cells at different timepoints during exit from naïve pluripotency. The first peak of ERK activation is likely a direct effect of the removal of the inhibitors. The timing of the second peak approximately coincides with the timing of the decrease in membrane tension and cell spreading (N=5). Inset, data for T16 and T20 cells where values for WT and iEZR_CA in individual experiments are connected by a line (N=5). **B**, Similar as panel a, for phospho-ERK normalised to total ERK levels. **C**, Left, bar plot showing the average log₂ fold change over all ERK-activated (n = 1879) or ERK-suppressed (n = 2169) at each of the three time-points. P-values indicate if these averages are significantly different to averages over randomly selected genes (computed using permutation test with replacement). Right, heatmap of ERK-target genes, either suppressed or activated during exit from naïve pluripotency (see methods for details). Colormap indicates the log₂ fold change between expression in iEZR_CA compared to wild-type cells. For both subsets (suppressed or activated), the top 50 genes are shown (sorted based on magnitude of Erk-regulation in wild-type cells at T24). **D**, Quantification of the percentage of surviving replated cells in a clonogenicity assay using WT T48 and iEZR_CA T48 cells treated with 3µM BI-D1870. Cells replated directly from 2i+L are used as a positive control (N=6). **E**, Representative single z-plane images of a mixed population of WT and iERC_CA (positive in the mCherry channel) T24 cells, immunostained for Fgfr1. **F**, Quantification of average intracellular Fgfr1 levels in T24 cells across different conditions (N=3). **G**, Fluorescent Western blot (inverted contrast) for Fgfr1 and GAPDH in WT and iEZR_CA ES and T24 cells, and corresponding quantification (data are normalised to GAPDH). (N=3). **H**, Top, representative images of z projections of fixed ES cells in different conditions. Bottom, associated quantification of FRET ratio for each condition. P values are calculated by Welch's unpaired student t-test using ES cells as reference. PD03 was used at 1 µM. Dynasore was used at 10 µM. Displayed pictures have been smoothed (Gaussian blur). P-values are calculated by Welch's unpaired student t-test (unless specified otherwise). Graphical data represents mean ± SD unless specified otherwise. Scale bars = 10 µm.